Nuclear Instruments and Methods in Physics Research A 338 (1994) 467–497
North-Holland

NUCLEAR
INSTRUMENTS
& METHODS
IN PHYSICS
RESEARCH
Section A

Signal processing considerations for liquid ionization calorimeters in a high rate environment **

W.E. Cleland *, E.G. Stern [1]

Department of Physics and Astronomy, University of Pittsburgh, Pittsburgh, PA 15260, USA

(Received 13 July 1993)

We present the results of a study of the effects of thermal and pileup noise in liquid ionization calorimeters operating in a high luminosity environment. The method of optimal filtering of multiply-sampled signals to obtain timing and amplitude from calorimeter signals is described. This method has some advantages over the traditional method of sampling the peak of a shaped signal, which include a reduced sensitivity to channel-to-channel variations in the pre-filter shaping parameters and good performance over a wide range of operating conditions. Analytic expressions for the variance of amplitude and timing measurements are found through a frequency domain approach. Implications for the choice of pre-filter shaping time, number and position of the samples, and digitization accuracy are discussed.

1. Introduction

We describe a technique for the determination of the amplitude and timing information of a shaped signal from a liquid ionization detector of the type typically used in high energy physics. In particular we wish to concentrate on the effects of distortion of the signal due to thermal noise and to real signals from uncorrelated events which are close in time to the event of interest, the "pileup" or "physics" noise. The proper choice of the shaping function permits optimal determination of the amplitude with a single measurement at the peak of the signal. However, because of channel-to-channel variations in the physical parameters which determine the optimal shaping time and because of practical limits on the production of shaping circuits of a given shaping time in high channel count applications, it is often necessary to work with non-optimal shaping. However, by multiply sampling the waveform and combining the samples in an optimal way, it is possible to achieve accuracy which exceeds that of a single sample, even though the actual shaping circuit may be far from optimal. In addition, the same samples may be combined with a different set of coefficients to obtain timing information.

The general approach for the determination of amplitude and timing from the samples is that of optimal filtering [1]. This method uses the autocorrelation function of the samples, which is a function of the ratio of the thermal to pileup noise amplitudes, to maximize the signal/noise ratio for determination of the time origin and the amplitude of the signal. The method has been tested by using Monte Carlo data, in which the distribution of pileup noise used is that obtained from ISAJET, a commonly used high energy physics event generator.

The motivation for this study is the need to understand such questions in designing signal processing electronics for liquid ionization calorimeters at high luminosity colliders, such as SSC and LHC. Practical considerations limit the peaking time of shaped signals to 20 ns or greater, and the entire waveform will dwell for at least as long as the drift time of the electrons in the detector planes, typically 400 ns. The colliders in question will have collisions at intervals much shorter than the dwell time, and hence pileup effects will occur. Because of the possibility of a collision occurring at each beam crossing (16 ns for the SSC), it may be necessary to sample the waveform at the frequency of beam crossings. Samples may be discarded, if the trigger logic in the experiment indicates that they are

[1] Present address: Nevis Laboratories, Columbia University, Irvington, NY, USA.

* Corresponding author.

** This manuscript has been authored under contract number DE-AC02-80ER10667 and Grant No. DE-FG02-90ER40646 with the US Department of Energy. Accordingly, the US Government retains a non-exclusive, royalty-free license to publish or reproduce the published form of this contribution, or allow others to do so, for US Government purposes.

SSDI 0168-9002(93)E0842-G

associated with an uninteresting event. Even for interesting events, it may not be necessary to digitize all samples; one only needs to preserve enough samples to accurately reconstruct the amplitude, timing, and waveform quality information.

In liquid ionization calorimeters with well designed signal processing electronics, parallel white noise and $1/f$ noise are negligible in comparison to series white noise [2]. The two principal sources of noise which must be considered for liquid ionization calorimeters operating in a high luminosity environment are therefore (1) series thermal noise, which has a white spectrum and whose amplitude depends only upon the characteristics of the detector and the signal processing circuitry; and (2) pileup or physics noise, which is due to the constant bombardment of calorimeter cells by products of collision reactions with high cross sections (mainly minimum bias and two jet events). Pileup signals are generated at a beam crossing frequency, and the number spectrum of the events is given by a Poisson distribution, whose mean value $\mathscr{N}_i$ for event type i is related to the cross section σ_i, the bunch spacing T_c, and the collider luminosity $\mathscr{L}$ by the simple formula $\overline{\mathscr{N}}_i = \mathscr{L} T_c \sigma_i$. For this reason the level of pileup noise depends on the luminosity $\mathscr{L}$ of the machine, which may vary with time. The level of pileup noise also depends on the depth of the calorimeter section, as deeper parts of the calorimeter are shielded from low energy particles. Because the transverse momentum spectrum is approximately independent of pseudorapidity η ($\eta = -\ln \tan \theta/2$, in which θ is the polar angle of the calorimeter cell with respect to the beam line), the pileup noise amplitude, when expressed in units of transverse energy, is a slowly varying function of η in the central region, $|\eta| \leq 3$. For the case $|\eta| > 3$, where tower size become comparable to or smaller than the sizes of showers in the calorimeter, special considerations apply which are studied elsewhere [3]. Although thermal noise depends only on the calorimeter geometry and the signal processing circuitry, because we work in units of transverse energy, all signals from the calorimeter are weighted with $\sin \theta$, so the thermal noise becomes negligible at large $|\eta|$.

We begin in section 2 with a brief discussion of the signal waveforms and how they are calculated. In section 3 we discuss the two major sources of noise and report the results of a study of the amplitude of the pileup noise expected at the SSC, including its variation with calorimeter tower size and depth. Section 4 contains a discussion of how these noise sources contribute to the resolution of the calorimeter. Assuming that multiple samples of the shaped signal will be taken, we introduce the notion of optimal filtering in the treatment of these samples. In section 5 we discuss the implications these studies have on the design of the data acquisition system for a large calorimeter. The method of optimal filtering is illustrated in section 6 by means of a Monte Carlo calculation. We summarize our results in section 7 and state the principal conclusions of the paper. Preliminary reports of this work have appeared elsewhere [4,5].

2. Signal waveforms

The waveforms to be analyzed in this paper are those produced by the convolution of the current waveform from the liquid ionization chamber with the impulse response of the circuit in the electronics chain, which we call the "pre-filter". The latter is described in a lumped parameter circuit model. A charge integrating preamplifier with feedback capacitance C_F is followed by an analog filter, which we assume to be of the form $(CR)^2 - (RC)^n$ with equal time constants $\tau_F = RC$ for the integration and differentiation stages. There is an additional stage of integration at the preamplifier input with time constant τ_A. For this system the response function is [6]

$$H(\omega) = \frac{K(j\tau_F\omega)^2}{(j\omega C_F)(1+j\tau_A\omega)(1+j\tau_F\omega)^{n+2}}. \qquad (1)$$

The δ-response of the pre-filter $h(t)$ is the Fourier transform of this function, with the normalization constant K chosen so that the peak of the first lobe is unity. The current for the liquid ionization chamber, assuming no recombination, is a linearly decreasing function of time:

$$i(t) = \frac{N_e q_e}{t_d}\left(1 - \frac{t}{t_d}\right) \qquad (0 \leq t \leq t_d), \qquad (2)$$

in which N_e is the number of electrons generated in the gap and q_e is the electronic charge.

The convolution of the current waveform with the impulse response yields the final signal waveform:

$$g(t) = \frac{1}{q_s} h(t) \star i(t) = \frac{1}{q_s}\int_{-\infty}^{\infty} i(t-u)h(u)\,du, \qquad (3)$$

in which q_s, the integrated signal charge, is the constant required to make the first lobe of $g(t)$ equal to unity.

A useful quantity which characterizes the impulse response is the measurement time t_m, defined as [7]

$$t_m = \int_0^{\tau_{zc}} h(t)\,dt \qquad (4)$$

and represents the effective time of integration of the current. In this expression τ_{zc} is the zero-crossing point of the first lobe of the impulse response, as indicated in Fig. 1. The ratio of charge q_s in the signal to the

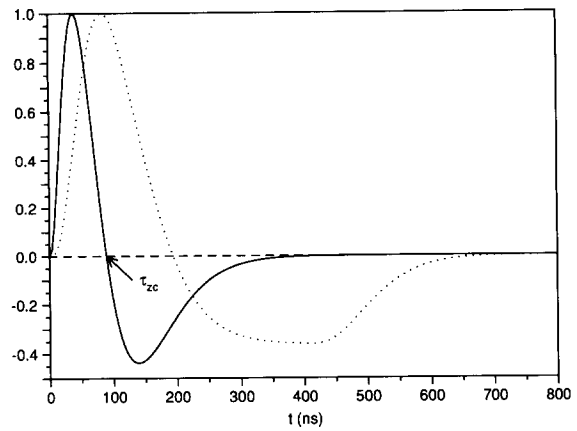

Fig. 1. Shape of the impulse response and the signal waveform for the standard case ($t_m = 50$ ns, $(RC)^2-(CR)^2$ shaping, $t_d = 400$ ns) used in this paper. The point marked τ_{zc} is used in the calculation of the measurement time t_m (see Eq. (2.4)).

charge of the electrons generated in the gaps is related, to a good approximation, to t_d and t_m by [7]:

$$r_q = \frac{q_s}{q_e N_e} \approx \frac{t_m}{t_d} - \frac{1}{2}\left(\frac{t_m}{t_d}\right)^2. \tag{5}$$

A parameter which is convenient for experimental use if the peaking time of the waveform t_p, defined to be the time taken for the signal to rise from 5 to 100% of the value of the first lobe. The relationship between t_m and t_p depends on the type of pre-filter used. The results in this paper are given in terms of t_m, in order to minimize dependence on the type of pre-filter chosen. For convenience, we give in Table 1 the relationship between t_m and t_p for three types of filters, along with the values of two quantities I_1 and S_p used throughout this paper. In calculating these values and throughout, we assume an amplifier time constant τ_A of 2 ns and a drift time t_d of 400 ns.

An illustration of the resulting waveforms for the case $t_m = 50$ ns and $t_d = 400$ ns with a $(CR)^2-(RC)^2$ pre-filter is shown in Fig. 1. We will use this waveform in various numerical examples in this paper, referring to our *standard case*, which is an EM tower of area $\Delta\eta\Delta\phi = 0.04 \times 0.04$, located 75 cm from the interaction point.

3. Noise sources

In this section we treat the two sources of noise which are important for the problem, and in each case we use a form which conveniently (for our purposes) separates that part of the amplitude which is dependent on the signal processing parameters from that part which depends on physical processes. In each case we refer to this latter factor as the noise "density".

Table 1
Values of peaking time, I_1, and S_p for three different pre-filters, as a function of t_m, the quantity used in this paper to characterize the impulse response waveform. In calculating these values, an amplifier time constant τ_F of 2 ns and a drift time t_d of 400 ns have been used

t_m [ns]	$(CR)^2-(RC)^2$			$(CR)^2-(RC)^4$			$(CR)^2-(RC)^6$		
	t_p [ns]	I_1 [ns^{-1}]	S_p [ns]	t_p [ns]	I_1 [ns^{-1}]	S_p [ns]	t_p [ns]	I_1 [ns^{-1}]	S_p [ns]
15	12.2	0.2039	28.9	13.3	0.2253	24.9	14.7	0.2411	24.3
20	15.3	0.1524	39.0	17.2	0.1588	33.8	19.0	0.1688	31.5
25	18.2	0.1230	49.5	21.4	0.1279	43.1	23.2	0.1351	40.1
30	21.2	0.1031	60.2	25.5	0.1079	52.3	27.5	0.1147	48.7
35	24.2	0.0889	71.1	29.4	0.0912	61.6	31.9	0.0967	57.5
40	27.4	0.0781	82.1	33.2	0.0801	71.4	36.2	0.0846	66.7
45	30.5	0.0698	93.2	37.5	0.0715	81.4	40.7	0.0758	75.8
50	33.7	0.0630	104.4	41.5	0.0640	91.2	45.0	0.0677	85.3
60	40.1	0.0527	126.4	49.6	0.0535	111.3	54.0	0.0567	104.4
70	46.6	0.0451	147.7	57.7	0.0458	131.6	62.9	0.0484	123.8
80	53.1	0.0395	168.2	65.9	0.0401	151.5	71.9	0.0423	143.2
90	59.6	0.0351	187.1	74.1	0.0357	170.7	80.8	0.0377	162.3
100	66.2	0.0317	204.9	82.2	0.0321	189.2	89.7	0.0339	181.0
120	79.4	0.0264	236.2	98.6	0.0267	223.2	107.6	0.0282	216.0
140	92.6	0.0226	262.7	115.0	0.0229	253.1	125.5	0.0242	247.3
160	105.7	0.0198	285.4	131.4	0.0201	279.2	143.4	0.0212	275.2
180	118.9	0.0176	305.2	147.8	0.0178	302.3	161.3	0.0188	300.2
200	132.1	0.0159	323.1	164.2	0.0160	323.1	179.2	0.0169	322.8

3.1. Thermal noise

The electronic noise is expressed as the equivalent noise charge at the input of the preamplifier. For the case in which the capacitance of the preamplifier is not matched to the ionization chamber gap capacitance the relationship for the equivalent noise charge due to series noise is [2]

$$\overline{\mathrm{ENC}^2} = \tfrac{1}{2} e_n^2 C_{tot}^2 I_1, \tag{6}$$

in which e_n is the series noise voltage density for the amplifier, C_{tot} is the sum of the detector capacitance and the channel capacitance of the transistor at the amplifier input, and I_1 is the series noise integral, which is related to the δ-response of the circuit $h(t)$ as:

$$I_1 = \int_{-\infty}^{\infty} \left(\frac{\mathrm{d}h}{\mathrm{d}t} \right)^2 \mathrm{d}t. \tag{7}$$

To express the noise in units of energy measured in the calorimeter, we calculate the charge generated by a particle of energy E_0 incident on the front face. The fraction of ionization energy deposited in the ionization gaps for a minimum ionizing particle is the sampling fraction η_s. Due primarily to the higher Z materials used in the absorber plates, the fraction of energy lost in the absorber for showering particles exceeds the value of $1/\eta_s$ by a factor a_e (the μ/e ratio). Therefore the energy E_g deposited by the showering particles is given by

$$E_g = E_0 \eta_s / a_e, \tag{8}$$

and the charge of the electrons generated by this energy is given by

$$q_e N_e = q_e E_g / W_{ion}, \tag{9}$$

in which W_{ion} is the mean energy required to create an ion pair in the liquid. Only a fraction $r_q = q_s / q_e N_e$ of these electrons are integrated in the signal, so the integrated number of signal charges becomes

$$q_s = r_q q_e \eta_s E_0 / a_e W_{ion}. \tag{10}$$

The scale factor needed to convert the noise from charge units to energy units is q_s/E_0, which leads to the following expression for the series thermal noise:

$$\sigma_t = \mathrm{ENC}/(q_s/E_0) \tag{11}$$

$$= \frac{1}{\sqrt{2}} \frac{e_n C_{tot} W_{ion} a_e}{\eta_s q_e r_q} \sqrt{I_1} = \frac{\rho_t}{r_q} \sqrt{I_1}. \tag{12}$$

We have separated the above expression into two factors: ρ_t, the thermal noise density, which is independent of the signal processing parameters, and the other, $\sqrt{I_1}/r_q$, which is independent of all of the calorimeter constants except for t_d. The dimensions of ρ_t are $E\sqrt{T}$. We give here, for reference, the values of the constants used in the above equations for the thermal noise density. We assume a sampling fraction η_s of 0.25, a μ/e ratio $a_e = 1.4$, and a total capacitance of 600 pf. The value of W_{ion} for liquid argon is 23.6 eV, and $q_e = 1.6 \times 10^{-19}$ C. The resulting value for the thermal noise density is $\rho_t = 8$ MeV $\sqrt{\mathrm{ns}}$, which is typical for a 3×3 cm^2 cell of a liquid argon calorimeter in the accordion geometry with a 2 mm gap and 25 radiations length deep.

3.2. Pileup noise

The problem of the effects of overlapping events at a high luminosity collider has received considerable attention in workshops for the SSC and LHC [10–13]. Early estimates were concerned with the random noise level seen in individual calorimeter cells, and the assumption was frequently made that noise from neighboring cells is independent and therefore may be added in quadrature. However, we know that a significant fraction of the pileup will come from two jet events since the cross section for their production is about half of the total cross section. In such events, the energy in neighboring cells will be correlated, due to the energy flow characteristics of jet events. As discussed below, we have evaluated this effect in a Monte Carlo calculation based on high cross section events and find that over a very wide range of area, the variance of the energy deposited in a given area scales as $\mathscr{A}^{0.76}$ at SSC energies. In this paper we work in angular space defined by the pseudorapidity η and the azimuth ϕ, and an area in this space is a cell of lateral dimensions $\mathscr{A} = \Delta\eta \times \Delta\phi$.

3.2.1. Pileup in time-variant systems

Pileup noise is a relatively new phenomenon in high energy physics. Typically, accidental backgrounds in high energy physics experiments are treated as individual events which must be subtracted from the desired signal. For calorimeters operating at high energy and high luminosity, however, the rate of particles striking the calorimeter is sufficiently high and their energy sufficiently low that it is more appropriate to classify this type of background as a noise source. In section 6 we address the question of whether an inherently non-Gaussian distribution is adequately represented by this treatment.

The focus of this paper is on liquid ionization calorimeters, which are normally handled by time-invariant techniques of shaping and sampling (the sampling introduces time-variance, but the essential elements of the signal processing are contained in the shaping, which is a time invariant process). In time-variant systems, such as gated integrators, the data processing is carried out numerically, and therefore a slightly different approach to the analysis of the system

is required. We include this discussion in the present paper, since there are certain common features in the two systems concerning the pileup noise. One such concept which is applicable to either system is that of the response function. This function plays an important role in the analysis of the time-invariant system, and we discuss below how the response function for a time-variant system may be similarly defined.

Let us imagine that we are dealing with a calorimeter whose output waveform is a δ-function: each time energy E_0 is deposited in the cell, the detector signal is $E_0\delta(t-t_0)$, in which t_0 is the time at which the interactions occur. We also assume that a certain amount of energy due to pileup events, on average, is deposited in the calorimeter at each beam crossing. Because the level of pileup depends on the luminosity $\mathscr{L}$ of the collider, which will vary with time, it will be important to establish continuously the amplitude of the pileup noise. One way would be to measure the pileup $\langle E\rangle$ in a narrow gate, so that only one crossing is detected. We assume that all particles produced in the interaction travel at velocity c, so that there is no overlap between events from different crossings. Let E_i be the instantaneous value present in crossing i. In this situation we measure the mean value of energy seen and its variance after N crossings:

$$\langle E\rangle = \sum_i E_i/N,$$

$$\sigma_E^2 = \frac{\sum_i E_i^2}{N} - \langle E\rangle^2 = \rho_p^2 T_c,$$

in which ρ_p, the symbol for pileup noise density, is introduced for comparison with the time-invariant case, and T_c is the period of the machine clock, or the time between bunch crossings. We now consider the situation where the gate is widened to a value of aT_c ($a>1$); the mean and variance measured with the wider gate are:

$$U = a\langle E\rangle,$$

$$\sigma_U^2 = a\sigma_E^2 = a\rho_p^2 T_c.$$

Now consider the case where a true signal of energy E_0 is present. We wish to measure this signal Q_i^a in a gate of width aT_c, but we need to subtract the pileup background. We sample the background at that instant in time by measuring the charge Q_i^b in a second gate of width bT_c.

The signal S calculated from the measured charge in the two gates is

$$S_i = Q_i^a - \frac{a}{b}Q_i^b = E_0 + U_i^a - \frac{a}{b}U_i^b$$

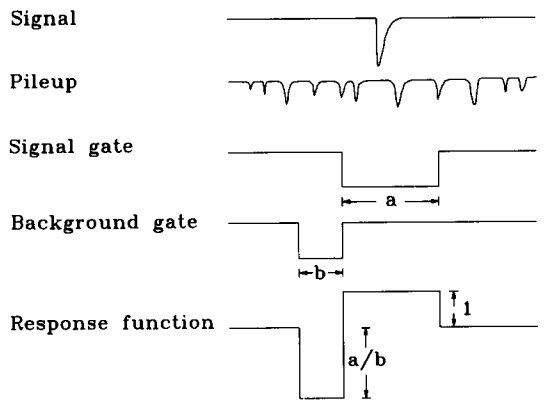

Fig. 2. Diagram showing the relative time of a signal and gates for an ideal calorimeter which is read into a gated integrator. The pileup noise is measured in the background gate, and the subtraction of the background from the signal, taking into account the different gate widths, results in the response for the system which is shown. It is the effective width of the response function that determines the level of pileup noise.

and the part of its variance due to the pileup is

$$\sigma_p^2 = a\rho_p^2 T_c + \left(\frac{a}{b}\right)^2 b\rho_p^2 T_c \tag{13}$$

$$= a\left(1+\frac{a}{b}\right)\rho_p^2 T_c. \tag{14}$$

We now calculate the response function $y(t)$ for this system. The response function is defined as the value of S for unit energy deposited at time t in the calorimeter cell. It takes on the following values:

$$y(t) = \begin{cases} 0 & t<-b \text{ or } t>a \\ -\dfrac{a}{b} & -b<t<0 \\ 1 & 0<t<a. \end{cases}$$

This function is illustrated in Fig. 2. The response function, when applied to the real input of the system and integrated over time is seen to be

$$\int_{-\infty}^{\infty} y(t)q(t)\,dt = \int_{-\infty}^{\infty} y(t)\left(E_0\delta(t)+E(t)\right)\,dt = E_0,$$

since the mean value of the pileup contribution $E(t)$ is zero. The effective width of the response function is defined as the width of a rectangle of unit height whose area is the integral of the square of the function:

$$W = \int_{-\infty}^{\infty} y^2(t)\,dt, \tag{15}$$

$$= \left(\frac{a}{b}\right)^2 bT_c + aT_c = aT_c\left(1+\frac{a}{b}\right).$$

Notice that the pileup variance can be expressed as

$$\sigma_p^2 = W\rho_p^2, \tag{16}$$

which is a useful property of the response function for the discussion of pileup noise. It is interesting to note that W is not simply the sum of the two gates, although $W = 2$ for the case $a = b$. If $b = a/2$, $W = 3a$, demonstrating the importance of the statistical factor $(a/b)^2$ in Eq. (13). From this example it can be seen that measuring the baseline in a gate narrower than that required for the signal would not be advantageous.

Because of the sensitivity to pileup, one could imagine *not* measuring the baseline in the second gate, but in this case it would be necessary to include in the variance any fluctuations in pileup noise due to variations in the luminosity, or, if the detector does not have a perfect δ-function output waveform (and no detector really does), there will be fluctuations in the baseline arising from the slower component of the response, which will also increase the variance. Both effects are removed by measuring the baseline in the second gate, but, as shown above, this procedure affects the sensitivity to pileup noise.

In summary, we see that the response function characterizes the signal processing operations of the system, and that its width, defined in Eq. (15) is a convenient parameter for describing the effects of signal processing on the contribution of pileup noise. In section 4 we calculate the response function for the time-invariant system.

3.2.2. Pileup in systems with bipolar shaping

In the situation where pileup noise is continuously distributed in time, Campbell's theorem [8–9] may be used to find the pileup variance. However, at a collider, where the signals are generated at fixed intervals, it is necessary to use a discrete sum in calculating the effect of pileup noise. The expression for this case is derived in the appendix.

From Eq. (99) we see that the expression for the pileup variance is

$$\sigma_p^2 = \rho_p^2 T_c \sum_{i=-\infty}^{\infty} g^2(t_i) = \rho_p^2 S_p \tag{17}$$

in which $\rho_p^2 = \mathrm{Var}(E)/T_c$ is the variance of the energy deposition in the calorimeter per crossing, T_c is the time between crossings, $g(t)$ is the signal waveform and S_p, called the "pileup sum" in this paper, is the discrete form of the so-called "pileup integral",

$$I_{2p} = \int_{-\infty}^{\infty} g^2(t)\,\mathrm{d}t. \tag{18}$$

The quantity ρ_p, called the pileup noise density, is that part of σ_p which is independent of the signal processing parameters. The dimensions of ρ_p are $E/\sqrt{T}$ while S_p has dimensions of T, reflecting the time interval over which pileup events contribute to the noise variance.

3.2.3. Monte Carlo evaluation of the pileup noise density

To estimate the effects of pileup, we use a Monte Carlo program to simulate the time structure of the machine by permitting collisions at points in time separated by the bunch crossing time and use Poisson statistics to determine the number of collisions of each type of events at each crossing. We consider only two jet (with transverse energy of the jet above 5 GeV) and minimum bias events, as generated in ISAJET version 6.21. The two types of events occur in approximately equal proportions.

Energy deposition in the calorimeter is simulated by the program [14] which employs the Bock parameterization [15] for the electromagnetic and hadronic showers. We assume a spherical calorimeter of inner radius 75 cm with two depth segmentations: an electro-magnetic section of thickness 25 radiation lengths and a hadronic section of 10 absorption lengths. Transverse spreading in the calorimeter is parameterized in a simple way, and comparisons with experimental data indicate that the width is correct to an accuracy of about 10%. In this calculation, we deal with sums of transverse energy, i.e. we assume that sin θ weighting is made immediately after the preamplifier.

After the transverse energy deposition for each calorimeter cell is determined, a sum for the cell E_i over all events in a given crossing is made. We calculate ρ_p by evaluating the quantity

$$\rho_p^2 = \frac{1}{T_c}\left[\frac{\sum_i E_i^2}{n} - \left(\frac{\sum_i E_i}{n}\right)^2\right], \tag{19}$$

which is a characteristic of the sample of events contributing to the pileup. We have calculated ρ_p for a range of values of the area of the calorimeter, from the size of individual cells ($\mathscr{A} = \Delta\eta \times \Delta\phi = 0.04 \times 0.04$) up to sizes comparable to or greater than that of jets. The results (see Fig. 3) leads one to the conclusion that

$$\rho_p \propto (\Delta\eta\Delta\phi)^{0.76}$$

over a wide range of tower sizes. For uncorrelated noise, one would expect the variance to be linear in $\mathscr{A}$; this result indicates that the correlations in energy deposits due to the dominance of jet production significantly alters this naive expectation. We can combine this scaling law, along with the obvious linear dependence of the pileup variance with luminosity, and using the absolute value of the curve shown in Fig. 3, we arrive at an empirical formula for the pileup noise density:

$$\rho_p = 380(\Delta\eta\Delta\phi)^{0.76}\left(\frac{\mathscr{L}}{\mathscr{L}_0}\right)^{1/2} \mathrm{MeV}/\sqrt{\mathrm{ns}}\,. \tag{20}$$

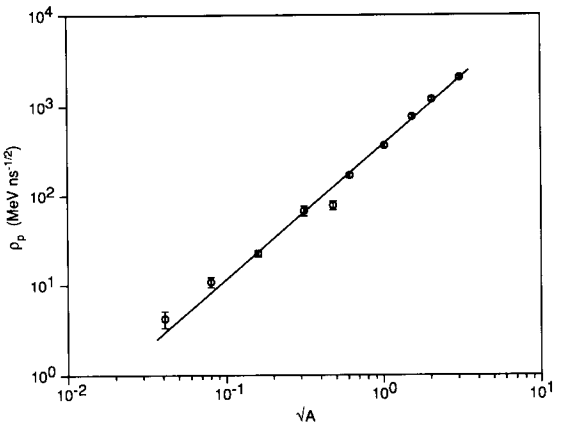

Fig. 3. Monte Carlo calculation of the pileup noise density $\rho_p = \sigma_p / \sqrt{S_p}$ found in a calorimeter tower as a function of the square root of its area $\mathscr{A} = \Delta\eta \otimes \Delta\phi$. For this calculation we have used ISAJET to generate 2 jet events, one of which has p_T in the range 5–10 GeV/c. In this calculation, the calorimeter is assumed to have spherical geometry, and the deposition is estimated using the Bock parameterization.

Very similar results have been obtained [16] using the Pythia event generator and a different parameterization for the deposition of energy in the calorimeter.

In this paper, the value of the pileup noise density ($\rho_p = 3.75$ MeV/$\sqrt{\text{ns}}$) used for our standard case corresponds to the data point for the cell of size 0.04×0.04.

4. Contribution of noise to calorimeter resolution

Because of the relatively short (≈ 16 ns) spacings between beam crossings and the high luminosity which leads to a collision rate of several events per crossing, the ability to correlate signals in time depends critically on the ability to extract the timing information form the signal itself. Intuitively, one expects that an improvement in timing resolution and a reduction in the effect of event pileup would be realized as the measurement time is decreased. However, such a reduction is accompanied by two effects which lead to a deterioration in the signal to noise ratio:

– The thermal noise increases as the bandwidth of the system is increased; the ENC is proportional to $1/\sqrt{t_m}$.

– As t_m is decreased, a smaller fraction ($= t_m/t_d$) of the charge deposited in the calorimeter is utilized in the signal processing, which leads to a reduction of the signal height, and since the noise is measured in energy units, a corresponding increase in the thermal noise.

Thus $\sigma_t \propto t_m^{-3/2}$, so t_m cannot be reduced to arbitrarily small values, and it cannot be increased to arbitrarily large values due to the effects of event pileup and degradation of the timing resolution. One of the main goals of this paper is to understand how to choose an optimum for the pre-filter shaping time t_m, considering the combined effects of thermal and pileup noise.

We approach the problem of determining the amplitude and timing information from a set of measured samples by looking first at the traditional method for extracting information from an overdetermined data set: the χ^2 method. We then turn to a solution from signal processing theory [1], optimal filtering, and show that the two methods are equivalent to first order. This equivalence is particularly relevant for online data processing since optimal filtering calculations are ideally suited for implementation in hardware using digital signal processors. We then discuss some implications of the optimal filtering formalism through the use of the system weighting and response functions. We have verified the method using Monte Carlo simulations of the noise signals by recovering the known input parameters of the signals with optimal filtering, as discussed in section 6.

We assume that the form of the signal at the output of the pre-filter is known, except for its amplitude A and time origin τ (the deviation from the assumed crossing time). The expression for this signal is

$$S_i = Ag(t_i - \tau), \tag{21}$$

in which g is the convolution of the impulse response $h(t)$ of the pre-filter with the drift current $i(t)$, as shown in Eq. (3). We also assume that the waveform will be sampled many times, giving a set of measurements $S_1, \cdots, S_n$. We wish to determine the parameters A and τ from the data set S_i.

4.1. χ^2 approach

We define the χ^2 function as follows:

$$\chi^2(A, \tau) = \sum_{ij} \big(S_i - Ag(t_i - \tau)\big) V_{ij} \big(S_j - Ag(t_j - \tau)\big) \tag{22}$$

in which V_{ij} is the weight matrix for the measured points S_i. The dependence on τ is linearized by the use of a Taylor expansion:

$$g(t_i - \tau) = g(t_i) - \tau g'(t_i),$$

in which $g'(t) = \mathrm{d}g/\mathrm{d}t$. Defining the two parameters in the fit to be $\alpha_1 = A$ and $\alpha_2 = A\tau$, we have

$$\chi^2 = \sum_{ij} \big(S_i - \alpha_1 g_i + \alpha_2 g_i'\big) V_{ij} \big(S_j - \alpha_1 g_j + \alpha_2 g_j'\big),$$

where we have adopted the obvious notational convenience that $g(t_i) = g_i$ and similarly for $g'(t_i)$. We now

form the following sums, expressed also in the equivalent matrix notation:

$$Q_1 = \sum_{ij} g_i V_{ij} g_j = \boldsymbol{g}^+ \mathbf{V} \boldsymbol{g},$$

$$Q_2 = \sum_{ij} g_i' V_{ij} g_j' = \boldsymbol{g}'^+ \mathbf{V} \boldsymbol{g}',$$

$$Q_3 = \sum_{ij} g_i' V_{ij} g_j = \boldsymbol{g}'^+ \mathbf{V} \boldsymbol{g},$$

$$Q_4 = \sum_{ij} g_i V_{ij} S_j = \boldsymbol{g}^+ \mathbf{V} \boldsymbol{S},$$

$$Q_5 = \sum_{ij} g_i' V_{ij} S_j = \boldsymbol{g}'^+ \mathbf{V} \boldsymbol{S}. \tag{23}$$

In these equations $\boldsymbol{g}$ is the line vector of the unit-amplitude shaping function samples, $\boldsymbol{g}^+$ is its transpose, and $\boldsymbol{g}'$ is its time derivative. The line vector $\boldsymbol{S}$ is the set of measured data points. We set $\partial\chi^2/\partial\alpha_i = 0$, and solve the resulting linear equations for α_i. The results are:

$$A \equiv \alpha_1 = \frac{1}{\Delta}[Q_2 Q_4 - Q_5 Q_3], \tag{24}$$

$$A\tau \equiv \alpha_2 = \frac{-1}{\Delta}[Q_1 Q_5 - Q_3 Q_4], \tag{25}$$

in which

$$\Delta = Q_1 Q_2 - Q_3^2.$$

The covariance matrix elements ϵ_{ij} for the parameters α_1 and α_2 are the elements of the inverse of the matrix $1/2\ \partial^2\chi^2/\partial\alpha_i\partial\alpha_j$:

$$\sigma_A^2 \equiv \epsilon_{11} = Q_2/\Delta, \tag{26}$$

$$A^2\sigma_\tau^2 \equiv \epsilon_{22} = Q_1/\Delta, \tag{27}$$

$$\epsilon_{12} = Q_3/\Delta. \tag{28}$$

In using this method, one normally solves the above equations, then recalculates the function with the new time parameter, and iterates the problem. This avoids errors due to the truncation of the Taylor expansion for g at the first term.

4.2. Optimal filtering in the time domain

In the context of calorimeter signal processing, optimal filtering refers to the formation of linear combinations of signal samples to recover the signal parameters, namely the amplitude A and start time τ, while minimizing the effects of noise. We define coefficients a and b and form the linear sums u and v of signal samples S:

$$u = \sum_i a_i S_i, \qquad v = \sum_i b_i S_i. \tag{29}$$

We will choose coefficients so that u will be the amplitude A of the signal, and v will evaluate to $A\tau$.

The shape of the signal is known, so that the samples S_i will have values

$$S_i = Ag(t_i - \tau) = Ag_i - A\tau g_i' + n_i,$$

where n_i is a noise component and use has been made of the Taylor series expansion as before. Since we require the expectation value of u to be A and the expectation value of v to be $A\tau$, we have

$$A = \langle u \rangle = \sum_i \left(Aa_i g_i - A\tau a_i g_i' + \langle n_i \rangle \right),$$

$$A\tau = \langle v \rangle = \sum_i \left(Ab_i g_i - A\tau b_i g_i' + \langle n_i \rangle \right).$$

The noise will average to 0, and this leads to constraints on a_i and b_i that

$$\sum_i a_i g_i = 1, \qquad \sum_i a_i g_i' = 0, \tag{30}$$

$$\sum_i b_i g_i = 0, \qquad \sum_i b_i g_i' = -1. \tag{31}$$

The variances of the parameters u and v are given by

$$\mathrm{Var}(u) = \sum_{ij} a_i a_j \langle n_i n_j \rangle = \sum_{ij} a_i a_j R_{ij},$$

$$\mathrm{Var}(v) = \sum_{ij} b_i b_j \langle n_i n_j \rangle = \sum_{ij} b_i b_j R_{ij}. \tag{32}$$

The expectation value $\langle n_i n_j \rangle = R_{ij}$ is the noise autocorrelation function evaluated at time $t_i - t_j$ which is discussed below in section 4.3.

We minimize the variances of u and v while satisfying the constraints of Eqs. (30) and (31) using Lagrange multipliers. The functions to be minimized are:

$$I_u = \sum_{ij} R_{ij} a_i a_j - \lambda\left(\sum_i a_i g_i - 1 \right) - \kappa \sum_i a_i g_i', \tag{33}$$

$$I_v = \sum_{ij} R_{ij} b_i b_j - \mu \sum_i b_i g_i - \rho\left(\sum_i b_i g_i' + 1 \right), \tag{34}$$

and λ, κ, μ and ρ are the Lagrange multipliers. Proceeding in the usual fashion and setting the partial derivatives with respect to a_i and b_i to 0 gives:

$$\frac{\partial I_u}{\partial a_i} = \sum_j R_{ij} a_j - \lambda g_i - \kappa g_i' = 0. \tag{35}$$

$$\frac{\partial I_u}{\partial b_i} = \sum_j R_{ij} b_j - \mu g_i - \rho g_i' = 0. \tag{36}$$

This is a set of linear equations which can be expressed in matrix form. In this form, the solution for $\boldsymbol{a} \equiv a_i$ and $\boldsymbol{b} \equiv b_i$ is:

$$\boldsymbol{a} = \lambda \mathbf{V} \boldsymbol{g} + \kappa \mathbf{V} \boldsymbol{g}', \tag{37}$$

$$\boldsymbol{b} = \mu \mathbf{V} \boldsymbol{g} + \rho \mathbf{V} \boldsymbol{g}'. \tag{38}$$

The matrix $\mathbf{V}$ is the inverse of the autocorrelation matrix $\mathbf{R} \equiv R_{ij}$ and is the same matrix that appears in Eq. (22) as the weight matrix of the signal samples.

The Lagrange multipliers can be determined from the constraint equations. For example, for λ and κ we have

$$\boldsymbol{g}\cdot\boldsymbol{a} = \lambda \boldsymbol{g}^{+}\mathbf{V}\boldsymbol{g} + \kappa \boldsymbol{g}^{+}\mathbf{V}\boldsymbol{g}' = 1,$$

$$\boldsymbol{g}'\cdot\boldsymbol{a} = \lambda \boldsymbol{g}'^{+}\mathbf{V}\boldsymbol{g} + \kappa \boldsymbol{g}'^{+}\mathbf{V}\boldsymbol{g}' = 0.$$

and similarly for μ and ρ with the constraints of Eq. (31). The solution in the notation of Eqs. (23) is

$$\lambda = \frac{Q_2}{\Delta}, \quad \kappa = \frac{-Q_3}{\Delta}, \tag{39}$$

$$\mu = \frac{Q_3}{\Delta}, \quad \rho = \frac{-Q_1}{\Delta}, \tag{40}$$

where $\Delta = Q_1Q_2 - Q_3^2$. Substitution of Eqs. (40) into Eqs. (37), (38) and (29) yields the same results as were given previously in Eqs. (24) and (25) for the general first order χ^2 method. Thus we see that the requirement of minimizing the variances of the parameters A and $A\tau$ and minimizing the χ^2 function to first order lead to the same results.

4.3. Covariance matrix for signal samples

Since we are dealing with a system which is bandwidth limited by the pre-filter, data samples taken in a time which is short compared to the dwell time of the shaped signal are correlated. It is necessary, when considering the treatment of highly correlated data, to understand the autocorrelation function for the system [17], from which we can obtain the covariance matrix for the data samples.

In our case, we have two sources of noise; thermal noise contributes a series noise and gives an autocorrelation function R_t, while pileup noise gives a parallel noise with an autocorrelation function R_p. These two autocorrelations are summed to give a total autocorrelation function.

$$\langle n_i n_j \rangle = R(t_i - t_j) = R_t(t_i - t_j) + R_p(t_i - t_j). \tag{41}$$

The function R_t is the series (thermal noise) autocorrelation function, given by

$$R_t(t) = \frac{\rho_t^2}{r_q^2}\int_{-\infty}^{\infty} h'(t+u)h'(u)\,\mathrm{d}u, \tag{42}$$

in which $h' = \mathrm{d}h/\mathrm{d}t$ and ρ_t is defined in Eqs. (11) and (12). The function R_p is the autocorrelation function for pileup noise:

$$R_p(t) = \rho_p^2 \int g(t+u)g(u)\,\mathrm{d}u. \tag{43}$$

Note that

$$R(0) = \sigma_t^2 + \sigma_p^2 = \sigma_s^2, \tag{44}$$

in which σ_s^2 is the variance of an individual sample S_i, σ_t is given by Eq. (12) and σ_p by Eq. (17).

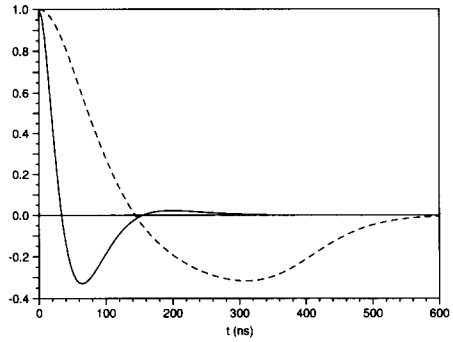

Fig. 4. Autocorrelation functions for series thermal noise (solid line) and pileup noise (dotted line). Both curves are normalized to unit amplitude. The total autocorrelation function is the sum of the solid curves multiplied by the thermal noise variance σ_t^2 and the dotted curve multiplied by the pileup noise variance σ_p^2. The autocorrelation function is symmetric in time, so these curves apply to $-t$ as well as t.

In Fig. 4 we show an example of $R_t(t)$ and $R_p(t)$ for our standard case ($t_m = 50$ ns, $t_d = 400$ ns). Note that R_p is a much wider function than R_t, which is due primarily to the fact that the function $g(t)$ is considerably wider than $h(t)$ because of the convolution with $i(t)$ (see Eq. (3)).

4.4. Weighting and response functions

In order to understand the implications of the solutions found above, we calculate here the weighting functions (one for each parameter) for the system as well as the response functions, which are closely related. The general definition of the weighting function [2] is the contribution to the system output at measurement time t_0 due to a unit impulse applied to its input at some previous time t. For a time-invariant system with impulse response $h(t)$, the weighting function is the mirror image of the impulse response, i.e. $w(t) = h(t_0 - t)$. Thus the weighting function can be viewed as a description of the memory of the system. For a system in which multiple samples are taken, each sample records a signal which contains the memory of the system relative to the time of that sample. Therefore if the signal reconstructed from the samples is of the form

$$A = \sum_i a_i S(t_i),$$

the weighting function for this system is given by

$$w_A(t) = \sum_i a_i h(t_i - t).$$

The composite weighting function for a set of 5 samples (pattern B, described below) is illustrated in Fig. 5.

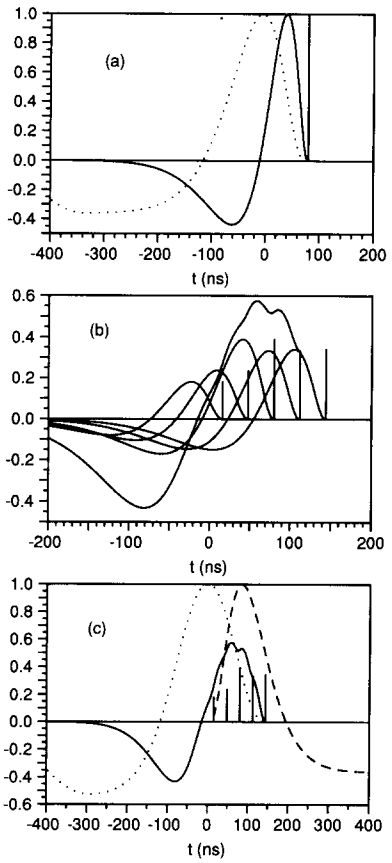

Fig. 5. Construction of the composite weighting and response function. (a) weighting function (solid curve) and response function (dotted) curve for a single sample with a coefficient a of unity. These are mirror images of the functions $h(t-t_s)$ and $g(t-t_s)$ about the time t_s of the sample. (b) Composite weighting function for the case of 5 samples (pattern B), found by multiplying each individual weighting function by the coefficient of the sample, which is indicated by the height of the vertical bar. (c) Solid curve: weighting function, as found in (b); dotted curve: response function, found in a similar way by combining the individual response functions: dashed curve: signal waveform. As in (b), the position of the vertical bars show the position of the samples, and their height indicates the values of the coefficients.

The response function is the contribution that a δ-function of *charge in the calorimeter* at time t makes to the output at time t_0. It is related but not identical to the weighting function, since in this case, the input to the preamplifier is not a δ-function but the current waveform (Eq. (2)), and the output waveform is $g(t)$. The amplitude response function describes the memory of the system, including the effects of drift time in the calorimeter. It is composed of a linear sum of the output waveforms:

$$y_A(t) = \sum_i a_i g(t_i - t). \tag{45}$$

This amplitude response function (or simply "response" function, except in cases where it is important to distinguish between the functions for amplitude and timing measurements) can be viewed as a measure of the response of the system to real signals which are out of time. Recalling Eq. (3), we see that $y_A(t)$ is the convolution of $w_A(t)$ with the current waveform

$$y_A(t) = w_A(t) \star i(t) = \int_{-\infty}^{\infty} i(t-u) w_A(u)\, du.$$

Fig. 5c shows both the weighting and response functions for the amplitude measurement for the case of sampling pattern B with five samples.

For the timing measurement, the weighting function $w_\tau(t)$ is defined in the same way, with the coefficients a_i replaced by the b_i. The timing response function $y_\tau(t)$ is similarly the convolution of $w_\tau(t)$ and $i(t)$. This gives

$$w_\tau(t) = \sum_i b_i h(t_i - t),$$

and

$$y_\tau(t) = \sum_i b_i g(t_i - t). \tag{46}$$

The timing response function has two properties which can be verified by inspection of the constraint equations Eq. (31). One is that $y_\tau(0) = 0$, and the other is that $y'_\tau(0) = -1$, so that the magnitude of the timing response function for a signal displaced by an amount τ is simply equal to τ. The curve of $y_\tau(t)$ vs t shows the region over which the optimal filtering method is able to determine the time offset. As is shown in section 4.6, $y_\tau(t)$ is proportional to $y'_A(t)$, which is a useful property for real time applications of optimal filtering.

We now consider the relationship between the variances of the parameters and properties of the response and weighting functions. Recall (Eq. (32)) that

$$\mathrm{Var}(A) = \sum a_i a_j R_{ij},$$

or

$$\sigma_A^2 = \sum a_i a_j R_t(t_i - t_j) + \sum a_i a_j R_p(t_i - t_j)$$
$$= \xi_t + \xi_p.$$

The quantities ξ_t and ξ_p are the contributions to the variance σ_A^2 coming from thermal and pileup noise, respectively.

By definition $y_A(0)$ is unity. The effective width of the response function, defined in Eq. (15), is

$$W = \int_{-\infty}^{\infty} y_A^2(t)\, dt = \int_{-\infty}^{\infty} \left[\sum_i a_i g(t_i - t) \right]^2 dt \tag{47}$$
$$= \sum_{ij} a_i a_j \int_{-\infty}^{\infty} g(u) g(t_j - t_i + u)\, du$$
$$= \frac{1}{\rho_p^2} \sum_{ij} a_i a_j R_p(t_i - t_j),$$

where the latter substitution comes from Eq. (43). We thus conclude that the pileup contribution of the variance is related to the effective width of the response function by the simple equation

$$\xi_p = \rho_p^2 W. \tag{48}$$

By comparison with Eq. (17), we see that the effective width of the response function W plays the same role as the integral I_{2p} plays for the variance of a single data point. Note the similarity between this expression and that derived for the simple case of a gated integrator (Eq. (16)).

The thermal noise for the case of multiple sampling can be viewed as a relation analogous to Eq. (12)

$$\xi_t = \frac{\rho_t^2}{r_q^2} I_1^{\text{eff}}, \tag{49}$$

in which I_1^{eff} is the integral over the square of the derivative of the composite weighting function:

$$\begin{aligned}\xi_t &= \frac{\rho_t^2}{r_q^2}\int_{-\infty}^{\infty} |w_A'|^2 \, dt \\ &= \frac{\rho_t^2}{r_q^2}\int_{-\infty}^{\infty} \left|\sum a_i h'(t_i - t)\right|^2 dt \\ &= \frac{\rho_t^2}{r_q^2}\sum a_i a_j \int_{-\infty}^{\infty} h'(u) h'(t_i - t_j + u)\, du \\ &= \sum a_i a_j R_t(t_i - t_j).\end{aligned}$$

From the arguments given at the beginning of this section, we know that σ_t scales as $t_m^{-3/2}$. Comparing Eq. (12) with Eq. (49) suggests that we can introduce an effective measurement time T for the multiply sampled system by requiring that it follows the same scaling law. We require that ξ_t vary as T^{-3} and that when $\xi_t = \sigma_t^2$ then $T = t_m$. This gives the relation

$$T = t_m\left(\frac{\sigma_t^2}{\xi_t}\right)^{1/3} = t_m\left(\frac{\sigma_t^2}{\sum a_i a_j R_t(t_i - t_j)}\right)^{1/3}.$$

For the timing measurement, we proceed in a similar way. First, we note that the variance for $A\sigma_\tau$ can also be written in terms of its thermal and pileup components:

$$\begin{aligned}&\text{Var}(A\tau) = \sum b_i b_j R_{ij}, \\ &A^2\sigma_\tau^2 = \sum b_i b_j R_t(t_i - t_j) + \sum b_i b_j R_p(t_i - t_j) \\ &\qquad = \zeta_t + \zeta_p.\end{aligned}$$

To define parameters with a physical interpretation, we consider the expression for the timing resolution for a system with a constant fraction discriminator operating at a point t_0 on the waveform $Eg(t)$ of amplitude E and normalized shape $g(t)$. If the noise in the system is σ_E, the time resolution is given by

$$\sigma_\tau = \sigma_E / E g'(t_0),$$

in which $g'(t_0)$ is the slope of the waveform at t_0. In the optimal filtering method, several points are measured on the waveform. We can, however, define an average effective slope m for the measurement, in analogy with the above expression:

$$m = \sigma_A / A\sigma_\tau.$$

We define two slope parameters m_t and m_p, which are the effective slopes in the thermal and pileup limits, respectively. In terms of the quantities defined above, they are given by

$$m_p = \sqrt{\xi_p / \zeta_p}$$

and

$$m_t = \sqrt{\xi_t / \zeta_t}.$$

These quantities have the useful property that they are independent of the value of ρ_t or ρ_p assumed in the calculation and depend only on the pre-filter shaping function and the sampling pattern assumed.

In summary, the four constants T, W, m_t, and m_p can be used to relate the values of σ_A and $A\sigma_\tau$ to the noise value for a single sample in the two limiting cases. In the case where thermal noise dominates

$$\sigma_A = \sigma_t\left(\frac{t_m}{T}\right)^{3/2} \quad \text{and} \quad A\sigma_\tau = \frac{\sigma_A}{m_t},$$

where σ_t is given by Eq. (12). In the limit where pileup noise dominates, we have

$$\sigma_A = \sigma_p\left(\frac{W}{S_p}\right)^{1/2} \quad \text{and} \quad A\sigma_\tau = \frac{\sigma A}{m_p},$$

where σ_p is given by Eq. (17).

In Fig. 6 we demonstrate one of the properties of the amplitude response function by showing how it behaves for two extreme cases: (1) the case for thermal noise only (i.e. $\rho_p = 0$) and (2) the case for pileup noise only ($\rho_t = 0$). In the first case, the response function maximizes its width, since there is no penalty for pileup, and the effective measurement time T is made as long as the pre-filter permits, thereby minimizing the thermal noise. In the second case, only pileup is important, so the effective width W becomes as small as possible, to minimize its effects. As is discussed in section 5.2, the limitation to the width of the amplitude weighting function in a practical system may be determined by the ADC quantization error.

4.5. Optimal filtering in the frequency domain

The optimal filtering problem can equivalently be considered in the frequency domain. Whereas in the

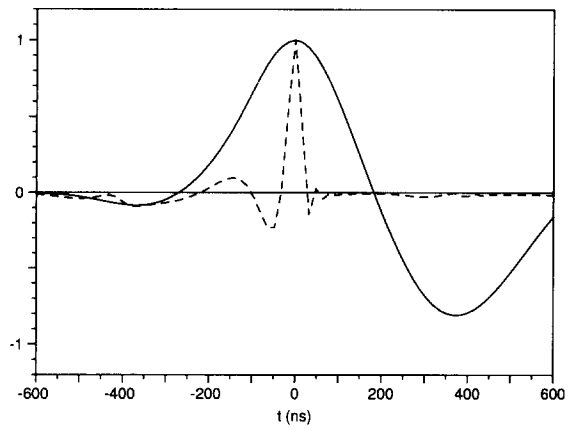

Fig. 6. Amplitude response function for two extreme cases: (1) dashed curve: pileup noise only (thermal noise = 0), (2) dotted curve: thermal noise only (pileup noise = 0). Note that if there is no pileup noise, the optimal filtering method broadens the weighting function (and hence the response function) in order to minimize the thermal noise. In the case where the thermal noise is negligible, the method minimizes the width of the response function in order to reduce the effects of pileup noise.

time domain, one has a known signal as a function of time and various noise sources, in the frequency domain, one has a signal with a known frequency spectrum, and noise sources with known spectra. The task is to develop a filter whose frequency response is such that it passes the signal frequencies but rejects noise frequencies.

The formalism for frequency domain filters is developed by Papoulis [1]. In the frequency domain, a filter is a function of frequency which multiplies the frequency distribution of the signal resulting in some new frequency distribution. The optimal filtering problem is to develop a filter which determines the unknown amplitude A and time offset τ of a signal which has the known form $Ag(t-\tau)$ in the presence of noise. We normalize the known signal $g(t)$ such that it has unit amplitude at its peak, and the problem then reduces to that of finding the value of the amplitude constant A with the highest signal/noise ratio.

It is shown in ref. [1] that for a signal with (complex) frequency spectrum $G(\omega)$, the Fourier transform of $g(t)$, and a noise power spectrum $S(\omega)$, the filter $\mathscr{H}(\omega)$ that maximizes signal/noise at time t_0 (the point in time at which the filter is optimized, which we choose to be 0) has a frequency response

$$\mathscr{H}_A(\omega) = \frac{K_A G^*(\omega)}{S(\omega)} e^{-j\omega t_0}, \tag{50}$$

where G^* is the complex conjugate of G and K_A is a multiplicative constant to normalize the filtered signal. This is the well-known matched filter, which intuitively has the right properties; it is large at frequencies where the signal is large and the noise is small, and it is small where the noise is large and the signal is small.

The filtered signal $y_f(t)$, is given by the inverse Fourier transform:

$$y_f(t) = \frac{1}{2\pi}\int_{-\infty}^{\infty} G(\omega)\mathscr{H}_A(\omega)\, e^{j\omega t}\, d\omega. \tag{51}$$

We wish to normalize the filter so that it gives unit amplitude for the peak when operating on the known waveform $g(t)$ with spectrum $G(\omega)$. This gives the condition that

$$\frac{1}{K_A} = \frac{1}{2\pi}\int_{-\infty}^{\infty} \frac{|G(\omega)|^2}{S(\omega)} d\omega. \tag{52}$$

Note that the exponential factors disappear since we are normalizing at the same point where the filter is optimized so the actual value of t_0 is unimportant. With this normalization, determination of the amplitude A of a signal waveform $u(t)$ with Fourier transform $U(\omega)$ is just

$$A = \frac{1}{2\pi}\int_{-\infty}^{\infty} \mathscr{H}_A(\omega)U(\omega)\, d\omega \tag{53}$$

$$= \frac{1}{2\pi}K_A\int_{-\infty}^{\infty} \frac{G^*(\omega)U(\omega)}{S(\omega)} d\omega. \tag{54}$$

The amplitude response function for the filter is the response of the filter to a signal of unit amplitude as a function of time shift. In the time domain, shifting the function $g(\tau)$ by amount t results in the function $g(\tau - t)$. In the frequency domain this time shift corresponds to multiplying the frequency spectrum $G(\omega)$ by the factor $e^{-j\omega t}$. Thus the response function is obtained by inserting for $U(\omega)$ in Eq. (53) the quantity $G(\omega)e^{-j\omega t}$ giving:

$$y_A(t) = \frac{1}{2\pi}\int_{-\infty}^{\infty} \mathscr{H}_A(\omega)G(\omega)\, e^{-j\omega t}\, d\omega. \tag{55}$$

Except for the sign of t, $\mathscr{H}(\omega)G(\omega)$ is the Fourier transform of the response function. Since $y_A(t)$ is a real function and equal to its complex conjugate, we can take the complex conjugate of the right hand side to identify $\mathscr{H}_A^*(\omega)G^*(\omega)$ as the Fourier transform of the response function $y_A(t)$. Using the expression for $\mathscr{H}_A$ from Eq. (50), we have

$$y_A(t) = \frac{K_A}{2\pi}\int_{-\infty}^{\infty} \frac{|G(\omega)|^2}{S(\omega)} e^{j\omega(t_0 - t)}\, d\omega. \tag{56}$$

We note that our normalization procedure gives the amplitude response function unit amplitude at $t = t_0$.

The spectral density of the filtered noise is $|\mathscr{H}_A|^2 S$ so the variance of the filtered signal is

$$\sigma_A^2 = \frac{1}{2\pi}\int_{-\infty}^{\infty} |\mathscr{H}_A(\omega)|^2 S(\omega)\,\mathrm{d}\omega$$
$$= \frac{1}{2\pi} K_A^2 \int_{-\infty}^{\infty} \frac{|G(\omega)|^2}{S^2(\omega)} S(\omega)\,\mathrm{d}\omega \qquad (57)$$
$$= K_A.$$

We now turn to the optimal filter for the time offset parameter τ. In this case, a change in the signal waveform $u(t)$ is related to τ through the derivative of g:

$$\delta u(t) = -A\tau g'(t).$$

Thus we proceed as before, only the filter is optimized for the Fourier transform of $-g'$, which is $-j\omega G(\omega)$. Therefore the optimal filter is

$$\mathscr{H}_\tau(\omega) = \frac{j\omega K_\tau G^*(\omega)}{S(\omega)} \mathrm{e}^{-\mathrm{j}\omega t_0}. \qquad (58)$$

We normalize the filter to give unity when presented with the Fourier transform of $-g'(t)$ evaluated at $t = t_0$:

$$1 = \frac{1}{2\pi}\int_{-\infty}^{\infty} \mathscr{H}_\tau(\omega)(-j\omega G(\omega))\,\mathrm{e}^{\mathrm{j}\omega t_0}\,\mathrm{d}\omega$$
$$= \frac{1}{2\pi}\int_{-\infty}^{\infty} \frac{K_\tau \omega^2 |G(\omega)|^2}{S(\omega)}\mathrm{d}\omega$$

or

$$\frac{1}{K_\tau} = \frac{1}{2\pi}\int_{-\infty}^{\infty} \frac{\omega^2 |G(\omega)|^2}{S(\omega)}\mathrm{d}\omega. \qquad (59)$$

With this normalization, for an unknown signal the value of $A\tau$ is

$$A\tau = \frac{1}{2\pi}\int_{-\infty}^{\infty} \mathscr{H}_\tau(\omega) U(\omega)\,\mathrm{d}\omega$$
$$= \frac{K_\tau}{2\pi}\int_{-\infty}^{\infty} \frac{j\omega G^*(\omega) U(\omega)}{S(\omega)}\mathrm{d}\omega. \qquad (60)$$

The response function for τ is the Fourier transform of the complex conjugate of the product of the filter and the signal function or

$$y_\tau(t) = \frac{K_\tau}{2\pi}\int_{-\infty}^{\infty} \frac{-j\omega |G(\omega)|^2}{S(\omega)} \mathrm{e}^{\mathrm{j}\omega(t_0 - t)}\,\mathrm{d}\omega. \qquad (61)$$

This product is purely imaginary and odd in ω, so the timing response function is real as it should be, and $y_\tau(t)$ is odd about t_0, which means that its value is 0 at $t = t_0$, as expected. Following the same reasoning used in Eq. (57), we find for the variance

$$\frac{1}{A^2\sigma_\tau^2} = \frac{1}{2\pi}\int_{-\infty}^{\infty} \frac{\omega^2 |G(\omega)|^2}{S(\omega)}\mathrm{d}\omega = \frac{1}{K_\tau}. \qquad (62)$$

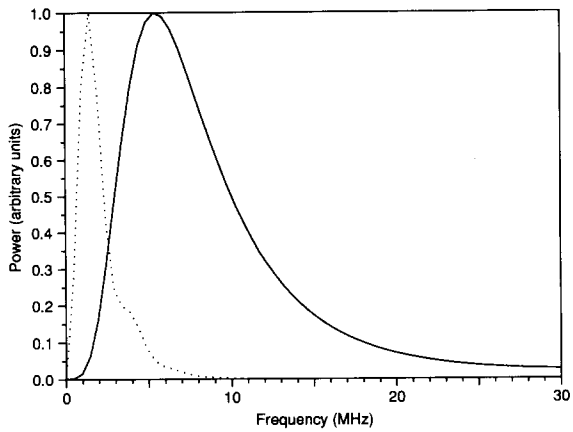

Fig. 7. Components of the power spectrum. The solid line is the curve for thermal noise and the dotted curve is the power spectrum for the pileup noise, which is also the spectrum for the signal. Each curve is normalized to unity. The optimal filter suppresses those frequencies outside of the signal region while preserving those frequencies where the signal is present.

From Eqs. (56) and (61) one sees that y_A and y_τ are related by

$$y_\tau(t) = \frac{K_\tau}{K_A} y_A'(t) = \left(\frac{A\sigma_\tau}{\sigma_A}\right)^2 y_A'(t) = \frac{y_A'(t)}{m^2}, \qquad (63)$$

as was mentioned in section 4.4. In this expression, m is the effective slope for the timing measurement introduced in section 4.4. It can also be easily verified from Eqs. (61) and (59) that at $t = t_0$, $y_\tau' = -1$, as required from its definition.

Multiplying the signal frequency spectrum with the frequency response of a filter corresponds in the time domain to a convolution of the signal with the Fourier transform of the filter response. Since the optimal filtering operation in the time domain as previously developed is formally a discrete convolution, we identify the coefficients a_i obtained earlier with the Fourier transform of the filter response $\mathscr{H}_A(\omega)$ obtained in the frequency domain using discrete Fourier transforms.

We have calculated the amplitude and timing optimal filters for our standard case, both in the time and frequency domain using discrete Fourier transforms. Fig. 7 shows the power spectrum of the two noise sources, pileup noise and thermal noise. The pileup noise comes from real events so it has the same spectrum as the signal. The thermal noise is represented as a current generator in parallel with the detector capacitance, so the noise δ-impulses are converted into δ' doublets [18]. The noise waveform is the convolution of the doublet with the pre-filter impulse response $h(t)$, which yields $h'(t)$, giving its power spectrum a larger high frequency component. We find very good agreement between coefficients given by the Fourier transform of a filter function with those calculated in the

time domain. For the purpose of this comparison, we assumed that the signal is sampled in a region symmetric around time zero in order to be consistent with the definitions used in the frequency domain calculation. Although there is negligible difference between the coefficients calculated by these two methods, the time domain allows more control over the number and position of samples (see section 5.3) making it more useful for practical purposes.

In the frequency domain, it is easy to understand the behavior or the amplitude response function in the two extreme cases described in section 4.4. Recall that the response function is $G(\omega)\mathscr{K}_A(\omega)$ where G is the signal frequency distribution and $\mathscr{K}_A$ is the filter spectral response. However, we know the form of $\mathscr{K}_A$ from Eq. (50), so the response function becomes proportional to $|G|^2/S$. For the case when $\rho_t \approx 0$ (negligible thermal noise), then the only contribution to $S(\omega)$ would be from pileup noise which has the same form as the signal power spectrum $|G|^2$. The response function is a constant in frequency space; the Fourier transform of a constant is a δ-function. Alternatively, for the case when pileup noise is negligible ($\rho_p \approx 0$), then the filter (and hence the response function) is only nonzero in a frequency band around the signal frequencies. The narrower the band, the wider its Fourier transform becomes.

4.6. Properties of optimal filters

Besides providing an intuitive understanding of optimal filters, the frequency domain formalism permits us to derive general properties of optimal filters that are not evident in the time domain formulation. As we have developed optimal filtering in the frequency domain, we have required integration over all frequencies. In the time domain, this corresponds to integration over all times and to sampling the signal at infinitely small time intervals. We refer to this unphysical situation as the "infinite sampling limit" (ISL). A situation somewhat closer to reality is found by integrating the function between fixed limits, which are determined in part by the sampling frequency and in part by the properties of the signal waveform. This represents the situation in which the signal is sampled periodically and a finite number of samples are analyzed. We refer to this situation as the "finite sampling". We give below the limits appropriate to performing the finite sampling integrals (FSIs) and derive analytic expressions for the variances of the parameters in this case. In a practical case of course, we must consider signals that are sampled at a few points located at integral multiples of the bunch crossing time. We show in section 5.3 the extent to which the infinite sampling limit formulae and finite sampling integrals approximate the practical situation.

We now derive analytic expressions for the variances of the parameters A and $A\tau$ in the infinite sampling limit. Consider an optimal filter which has as its input digitized data from a pre-filter with an impulse response $h(t)$. The impulse response spectrum $H(\omega)$ is the Fourier transform of $h(t)$. The signal waveform $g(t)$ is the convolution of $h(t)$ with the current waveform as discussed in Eq. (3). In the frequency domain, this means that the signal spectrum $G(\omega)$ is $I(\omega)H(\omega)/q_s$ where $I(\omega)$ is the Fourier transform of the current waveform $i(t)$. The factor $1/q_s$ appears because both $g(t)$ and $h(t)$ are normalized to unity. The noise spectral density $S(\omega)$ is a sum of the spectra $S_p(\omega)$ and $S_t(\omega)$ for pileup and thermal noise. Pileup noise is derived from real events so it must have a spectrum proportional to $|G|^2$. The integral of the pileup spectral density over all frequencies must equal the pileup variance:

$$\sigma_p^2 = \frac{1}{2\pi}\int_{-\infty}^{\infty} S_p(\omega)\,d\omega.$$

For the case of continuously distributed pileup, the variance is known from Campbell's theorem to be $\rho_p^2 \int g^2(t)\,dt$. From Parseval's theorem of Fourier analysis we also know that $\int g^2(t)\,dt = 1/2\pi \int |G(\omega)|^2\,d\omega$ so we obtain

$$S_p(\omega) = \rho_p^2|G(\omega)|^2 = \frac{\rho_p^2}{q_s^2}|I(\omega)|^2|H(\omega)|^2. \tag{64}$$

As mentioned above, representing the series noise as a parallel source introduces an effective differentiation in the spectrum, so the pre-filter response to thermal noise is proportional to $h'(t)$. The spectrum of $h'(t)$ is $j\omega H(\omega)$ so the thermal noise spectral density is proportional to $\omega^2|H(\omega)|^2$. Again using Parseval's theorem and noting the form of σ_t in Eq. (11) gives

$$S_t(\omega) = \frac{\rho_t^2\omega^2}{r_q^2}|H(\omega)|^2. \tag{65}$$

We now calculate σ_A^2, the variance of the amplitude after optimal filtering, using to Eq. (57) and recalling that $r_q = q_s/q_e N_e$:

$$\begin{aligned}\frac{1}{\sigma_A^2} &= \frac{1}{2\pi}\int_{-\infty}^{\infty}\frac{|G(\omega)|^2}{S_p(\omega)+S_t(\omega)}d\omega \\ &= \frac{1}{2\pi}\int\frac{\frac{1}{q_s^2}|I(\omega)|^2|H(\omega)|^2}{\frac{\rho_p^2}{q_s^2}|I(\omega)|^2|H(\omega)|^2+\frac{\rho_t^2\omega^2}{r_q^2}|H(\omega)|^2}d\omega \\ &= \frac{1}{2\pi}\int_{\omega\neq 0}\frac{\left(\frac{1}{q_e N_e}\right)^2|I(\omega)|^2}{\left(\frac{\rho_p}{q_e N_e}\right)^2|I(\omega)|^2+\rho_t^2\omega^2}d\omega.\end{aligned} \tag{66}$$

The point at $\omega = 0$ has been excluded because the noise and signal do not have any DC component, rendering the integrand undefined. Excluding this single point does not affect the integral.

The quantity $I(\omega)$ is the Fourier transform of the current waveform $i(t)$. For liquid ionization calorimeters [7] this is the linear function of time given in Eq. (2). The Fourier transform of this function is

$$\frac{I(\omega)}{q_e N_e} = \frac{1}{j\omega t_d} - \frac{2\, e^{-j\omega t_d/2} \sin\frac{\omega t_d}{2}}{j\omega^2 t_d^2},$$

from which we have

$$\frac{|I(\omega)|^2}{q_e^2 N_e^2} = \frac{1}{\omega^2 t_d^2} - \frac{4 \sin\frac{\omega t_d}{2}\cos\frac{\omega t_d}{2}}{\omega^3 t_d^3} + \frac{4 \sin^2\frac{\omega t_d}{2}}{\omega^4 t_d^4}. \tag{67}$$

Considering the integrand of Eq. (66)

$$\frac{\frac{a}{\omega t_d^2} + \frac{b}{\omega^3 t_d^3} + \frac{c}{\omega^4 t_d^4}}{\rho_p^2\left(\frac{a}{\omega^2 t_d^2} + \frac{b}{\omega^3 t_d^3} + \frac{c}{\omega^4 t_d^4}\right) + \rho_t^2\omega^2},$$

with a, b, and c values of magnitude less than 1, we see that at large ω, the terms proportional to b and c become small compared to the leading term proportional to a. At small ω, the term in the denominator proportional to ω^2 becomes small, and the integrand approaches $1/\rho_p^2$. Both of these conditions still hold if we approximate $|I(\omega)|^2/q_e^2 N_e^2$ by its first term $1/\omega^2 t_d^2$.

This leaves us with the expression

$$\frac{1}{\sigma_A^2} = \frac{1}{2\pi}\int_{-\infty}^{\infty} \frac{\frac{1}{\omega^2 t_d^2}}{\frac{\rho_p^2}{\omega^2 t_d^2} + \rho_t^2\omega^2}\, d\omega$$

$$= \frac{1}{2\pi}\int_{-\infty}^{\infty} \frac{1}{\rho_p^2 + \rho_t^2 t_d^2 \omega^4}\, d\omega \tag{68}$$

$$= \frac{1}{2\pi\sqrt{t_d \rho_t \rho_p^3}}\int_{-\infty}^{\infty} \frac{du}{1+u^4} \tag{69}$$

where we have made the substitution

$$u = \sqrt{\frac{t_d \rho_t}{\rho_p}}\,\omega. \tag{70}$$

The integral can be evaluated by contour integration and has the value of $\pi/\sqrt{2}$ leading to the variance for A in the infinite sampling limit:

$$\tilde{\sigma}_A^2 = \sqrt{8 t_d \rho_t \rho_p^3}. \tag{71}$$

All quantities calculated in the ISL are designated with a tilde ($\sim$).

The total filtered noise variance σ_A^2 has contributions from thermal and pileup noise

$$\xi_p = \frac{1}{2\pi}\int_{-\infty}^{\infty} |\mathscr{H}_A(\omega)|^2 S_p(\omega)\, d\omega,$$

$$\xi_t = \frac{1}{2\pi}\int_{-\infty}^{\infty} |\mathscr{H}_A(\omega)|^2 S_t(\omega)\, d\omega. \tag{72}$$

We write the noise spectral density (see Eqs. (64) and (65)) as

$$S(\omega) = \theta_p U_p(\omega) + \theta_t U_t(\omega),$$

where

$$S_p(\omega) = \rho_p^2 U_p(\omega) = \theta_p U_p(\omega),$$

$$S_t(\omega) = \rho_t^2 U_t(\omega) = \theta_t U_t(\omega).$$

From Eq. (72) the form for ξ_p, the contribution of pileup to σ_A^2, is

$$\xi_p = \frac{\frac{1}{2\pi}\int_{-\infty}^{\infty} \frac{|G(\omega)|^2}{S(\omega)^2} S_p(\omega)\, d\omega}{\left[\frac{1}{2\pi}\int_{-\infty}^{\infty} \frac{|G(\omega)|^2}{S(\omega)} d\omega\right]^2}$$

$$= \frac{\frac{1}{2\pi}\theta_p \int_{-\infty}^{\infty} \frac{|G(\omega)|^2}{\left(\theta_p U_p(\omega) + \theta_t U_t(\omega)\right)^2} U_p(\omega)\, d\omega}{\left[\frac{1}{2\pi}\int \frac{|F(\omega)|^2}{\theta_p U_p(\omega) + \theta_t U_t(\omega)} d\omega\right]^2}$$

$$= \theta_p \frac{\partial}{\partial\theta_p}\left(\frac{1}{2\pi}\int \frac{|G(\omega)|^2}{\theta_p U_p(\omega) + \theta_t U_t(\omega)} d\omega\right)^{-1}$$

$$= \theta_p \frac{\partial \sigma_A^2}{\partial \theta_p}, \tag{73}$$

and similarly for the thermal contribution. Identifying $\theta_p = \rho_p^2$ and $\theta_t = \rho_t^2$ and applying Eq. (73) gives us the pileup and thermal contributions in the ISL as

$$\tilde{\xi}_p = 3\sqrt{\frac{t_d \rho_t \rho_p^3}{2}} = \tfrac{3}{4}\tilde{\sigma}_A^2,$$

$$\tilde{\xi}_t = \sqrt{\frac{t_d \rho_t \rho_p^3}{2}} = \tfrac{1}{4}\tilde{\sigma}_A^2. \tag{74}$$

Note that these results are independent of any parameters of the impulse response function, such as the shaping time or order of the pre-filter.

The variance of the timing parameter $A\sigma_\tau$ can also be calculated the same way starting from Eq. (62) and

proceeding as before. After using the same approximation for the drift function, we have

$$\frac{1}{A^2\tilde{\sigma}_\tau^2} = \frac{1}{2\pi}\int_{-\infty}^{\infty}\frac{\omega^2\,d\omega}{\rho_p^2 + t_d^2\rho_t^2\omega^4} = \frac{1}{2\pi\sqrt{t_d^3\rho_t^3\rho_p}}\int_{-\infty}^{\infty}\frac{u^2\,du}{1+u^4}. \tag{75}$$

This integral also has the value $\pi/\sqrt{2}$ so

$$A^2\tilde{\sigma}_\tau^2 = \sqrt{8t_d^3\rho_t^3\rho_p}, \tag{76}$$

with thermal and pileup contributions

$$\tilde{\zeta}_p = \sqrt{\frac{t_d^3\rho_t^3\rho_p}{2}} = \tfrac{1}{4}A^2\tilde{\sigma}_\tau^2,$$

$$\tilde{\zeta}_t = 3\sqrt{\frac{t_d^3\rho_t^3\rho_p}{2}} = \tfrac{3}{4}A^2\tilde{\sigma}_\tau^2. \tag{77}$$

By comparing Eq. (48) with Eq. (74) we see that we can obtain a value for the effective width of the response function in the ISL:

$$\tilde{W} = \frac{3\sqrt{2}}{2}\sqrt{\frac{t_d\rho_t}{\rho_p}}. \tag{78}$$

The expression has the properties that one intuitively expects, namely that the effective width is increased as the thermal noise increases and decreases as the pileup noise increases. We note also that the effective slope for the timing measurement introduced in section 4.4 can be calculated in the ISL. We find

$$\tilde{m} = \sqrt{\frac{\rho_p}{t_d\rho_t}} = \frac{3\sqrt{2}}{2}\frac{1}{\tilde{W}}.$$

The degree to which the actual response functions follow these formulae is discussed in section 4.7.

Use of limits on the integrals which span all frequencies corresponds to sampling the waveform at infinitesimally spaced points extending over all time. It is this obviously unphysical sampling pattern which leads to the unphysical behavior of Eqs. (71) and (76) as either ρ_t or ρ_p approaches zero. We now show how our results are modified when sampling at finite intervals over a finite region of time is introduced.

We suppose that the signal waveform is sampled N times at sampling intervals T_s, which could be the machine crossing period T_c or some multiple thereof. The full width of the sampled region is therefore $\Delta = NT_s$. The effect of the finite sampling is to restrict the frequency range over which the signal processing network operates to a finite number of discrete frequencies given by:

$$\omega_k = k\Delta\omega, \quad \Delta\omega = 2\pi/\Delta, \tag{79}$$

where k has a range determined by the number of samples

$$k = -\frac{N}{2}, -\frac{N}{2}+1, \cdots, -2, -1, 1, 2, \cdots, \frac{N}{2}-1, \frac{N}{2}. \tag{80}$$

According to the Nyquist theorem, the largest angular frequency that can be distinguished given the sampling interval is $2\pi/2T_s$.

To estimate the variances of the parameters we utilize Eqs. (66) and (75), but apply finite limits:

$$\frac{1}{\sigma_A^2} = \frac{2}{2\pi\sqrt{t_d\rho_t\rho_p^3}}\int_{u_l}^{u_h}\frac{du}{1+u^4},$$

$$\frac{1}{A^2\sigma_\tau^2} = \frac{2}{2\pi\sqrt{t_d^3\rho_t^3\rho_p}}\int_{u_l}^{u_h}\frac{u^2\,du}{1+u^4}. \tag{81}$$

The values of these integrals from the Maple computer algebra program are:

$$\int\frac{du}{1+u^4} = \frac{\sqrt{2}}{8}\left[\log\frac{u^2+u\sqrt{2}+1}{u^2-u\sqrt{2}+1} + 2\tan^{-1}\left(u\sqrt{2}+1\right) + 2\tan^{-1}\left(u\sqrt{2}-1\right)\right],$$

$$\int\frac{u^2\,du}{1+u^4} = \frac{\sqrt{2}}{8}\left[\log\frac{u^2-u\sqrt{2}+1}{u^2+u\sqrt{2}+1} + 2\tan^{-1}\left(u\sqrt{2}+1\right) + 2\tan^{-1}\left(u\sqrt{2}-1\right)\right].$$

Note that the frequency ω is related to u by the equation $u = \omega/\omega_0$. Since $\omega_0 = \sqrt{\rho_p/\rho_t t_d}$, we see that in the case where pileup noise dominates u becomes small, and similarly, if thermal noise dominates, u becomes large. Therefore, the limits on the integrals may be found by requiring that the values of the integrals approach the values for the variances in these two limiting cases. We choose to establish them by evaluating σ_A^2 and $A^2\sigma_\tau^2$ for the two limiting cases. We therefore estimate ξ_t and ξ_p, the values of σ_A^2 for the case where either thermal or pileup noise dominates, respectively, and by using the limiting forms of the integrals, we relate these values to the integral limits $u_u = \omega_u/\omega_0$ and $u_l = \omega_l/\omega_0$. (We use the additional subscripts A and τ on the limits for the integrals for σ_A and $A\sigma_\tau$, respectively.) For the pileup noise limit the limiting form of the integral is

$$\lim_{u\to 0}\int\frac{du}{1+u^4} = u$$

and combining this with Eq. (69) we find

$$\frac{1}{\xi_p} = \frac{u_{A,u} - u_{A,l}}{\pi\sqrt{t_d \rho_t \rho_p^3}} = \frac{\omega_{A,u} - \omega_{A,l}}{\pi \rho_p^2},$$

which yields

$$\omega_{A,u} = \frac{\pi \rho_p^2}{\xi_p} + \omega_{A,l}.$$

Similarly, for the case where thermal noise dominates, the limiting value of the integral is

$$\lim_{u\to\infty} \int \frac{du}{1+u^4} = \frac{\pi}{2\sqrt{2}} - \frac{1}{3u^3}$$

and using Eq. (69) again we find

$$\frac{1}{\xi_t} = \frac{1}{3\pi\sqrt{t_d \rho_t \rho_p^3}} \left(\frac{1}{u_{A,l}^3} - \frac{1}{u_{A,u}^3} \right) \approx \frac{1}{3\pi t_d^2 \rho_t^2 \omega_{A,l}^3},$$

which yields

$$\omega_{A,l}^3 = \frac{\xi_t}{3\pi t_d^2 \rho_t^2}.$$

Similar considerations lead to the following expressions for the integral limits for $A\sigma_\tau$:

$$\frac{1}{\omega_{\tau,l}} = \frac{\pi \rho_t^2 t_d^2}{\zeta_t} + \frac{1}{\omega_{\tau,u}},$$

$$\omega_{\tau,u}^3 = \frac{3\pi \rho_p^2}{\zeta_p}.$$

The expressions for the parameter variances in terms of the integral limits are therefore:

$$\sigma_A = \begin{cases} t_d \rho_t \sqrt{3\pi \omega_{A,l}^3} & \text{(thermal region)}, \\ \left(8 t_d \rho_t \rho_p^3\right)^{1/4} & \text{(ISL region)}, \\ \rho_p \sqrt{\pi/(\omega_{A,u} - \omega_{A,l})} & \text{(pileup region)}. \end{cases} \quad (82)$$

and

$$A\sigma_\tau = \begin{cases} t_d \rho_t \sqrt{\pi/(1/\omega_{\tau,l} - 1/\omega_{\tau,u})} & \text{(thermal region)}, \\ \left(8 t_d^3 \rho_t^3 \rho_p\right)^{1/4} & \text{(ISL region)}, \\ \rho_p \sqrt{3\pi/\omega_{\tau,u}^3} & \text{(pileup region)}. \end{cases} \quad (83)$$

There are three separate approximations for each parameter: the thermal noise region applies when the luminosity is zero, or when pileup noise is very small compared with the thermal noise, and the pileup region applies when pileup is the dominant form of noise. Between these two regions, the ISL is a reasonably good approximation to the exact solution.

In the discussion in section 4.4, we have shown how the optimal filtering results for σ_A and $A\sigma_\tau$ can be expressed in terms of four quantities: the effective integration time T, the effective width of the response function W, and the two effective slopes m_t and m_p. From the expressions given here, it is straightforward to express the integral limits in terms of these parameters:

$$\omega_{A,l} = \left(\frac{I_1}{3\pi r_q^2 t_d^2} \right)^{1/3} \frac{t_m}{T},$$

$$\omega_{A,u} = \frac{\pi}{W} + \omega_{A,l},$$

$$\omega_{\tau,u} = \left(\frac{3\pi m_p^2}{W} \right)^{1/3},$$

$$\frac{1}{\omega_{\tau,l}} = \frac{m_t^2}{3\omega_{A,l}^3} + \frac{1}{\omega_{\tau,u}}.$$

With the integral limits, which represent the behavior of a system consisting of a given pre-filter shaping function and a given sampling pattern in the two limiting regions (thermal and pileup), it is possible to use the finite sampling integrals to obtain the values for σ_A and $A\sigma_\tau$ at any intermediate value of noise densities.

4.7. Numerical studies

We now illustrate the concepts that have been developed in the preceding sections, comparing the infinite sampling limit and the finite sampling integral with practical sampling scenarios. The data presented here are for the standard case of an EM 0.04×0.04 tower of the accordion type, although the qualitative behavior described is quite general. As mentioned in section 2, our estimates for an accordion-type liquid argon calorimeter lead to the following values for the calorimeter parameters: $\rho_t = 8$ MeV $\sqrt{\text{ns}}$ and $\rho_p = 3.75$ MeV/$\sqrt{\text{ns}}$ at $\mathscr{L} = 10^{33}$ cm^{-2} s^{-1}.

In order to see the effect of different choices of sampling pattern on the integral limits, we present an example of three sampling patterns (A, B, and C) of 5 samples each and the case for full sampling over the waveform (pattern D), with one sample at each beam crossing. The position of the three 5-sample patterns relative to the waveform are described in Table 2 and shown in Figs. 8 and 9, where we also show the weighting and response functions at two values of luminosity. Each of the patterns has the central sample near the peak of the waveform. In pattern A, every sample is taken, whereas in pattern B, every other sample is taken, and in pattern C, every third sample is taken. As can be seen in the figures, the sample spacing can have important consequences for the shape of the weighting functions, but the response functions are quite similar in shape. Sampling pattern D has a total of 44 samples, one each 16 ns, spread over the

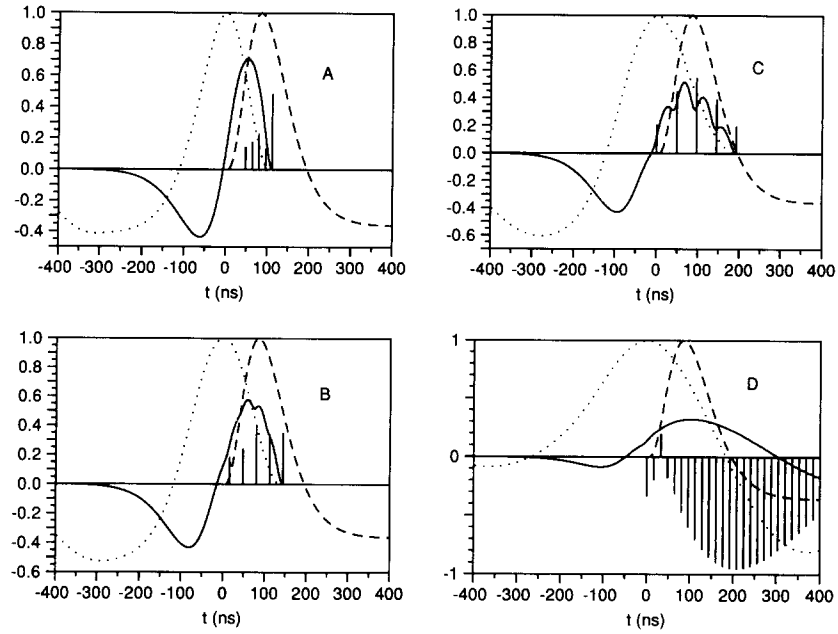

Fig. 8. Composite weighting function $w_A(t)$ and response function $y_A(t)$ for the amplitude measurement in the thermal noise limit. Solid curve: weighting function, dotted curve: response function, dashed curve: signal waveform. The four plots correspond to the four sampling patterns (A, B, C, and D) described in the text. The position of the samples is indicated by the horizontal position of the vertical bars, and the values of the corresponding coefficients a_i are indicated by the height of the bars. Note that $y_A(0) = 1$, as required by the constraints.

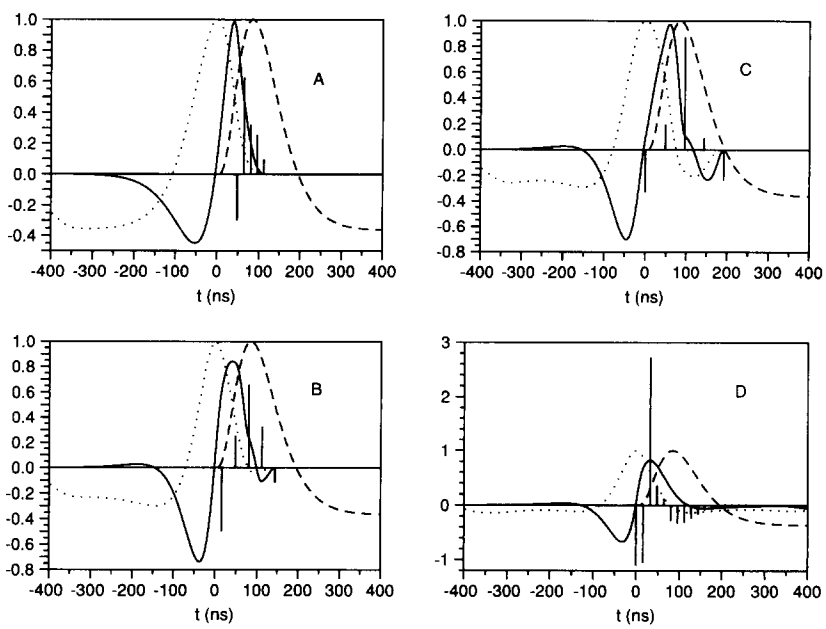

Fig. 9. Composite weighting and response function for the amplitude measurement for the standard luminosity. See Fig. 8 for details.

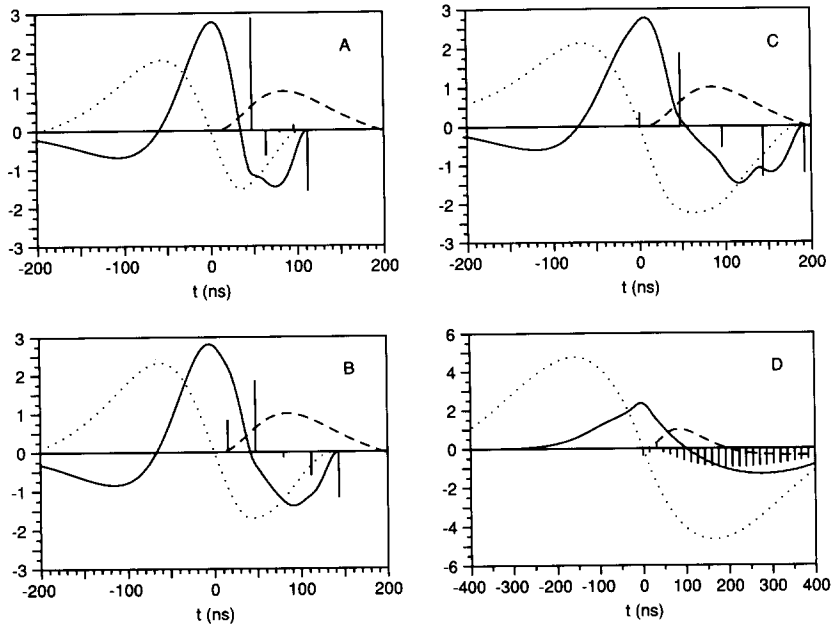

Fig. 10. Composite weighting function $w_\tau(t)$ and response function $y_\tau(t)$ for the timing measurement in the thermal noise limit. Solid curve: weighting function, dotted curve: response function, dashed curve: signal waveform. The four plots correspond to the four sampling patterns (A, B, C, and D) described in the text. The position of the samples is indicated by the horizontal position of the vertical bars, and the values of the corresponding coefficients b_i are indicated by the height of the bars. Note that $y'_\tau(0) = -1$, as required by the constraints. The units of y_τ are beam crossing periods (16 ns).

entire waveform. It is included here as the limiting case for a finite number of samples. The corresponding waveforms for the timing measurements are shown in Figs. 10 and 11.

In Table 3 we give the parameters T, W, m_p, and m_t, which characterize the sampling patterns for the limiting cases, along with the corresponding frequency limits for the integrals. One can see that full sampling

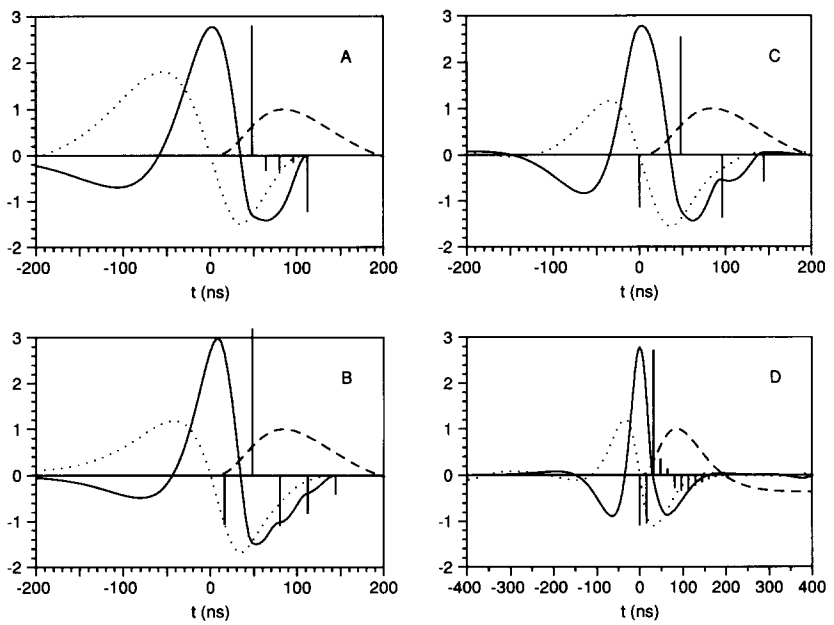

Fig. 11. Composite weighting and response function for the timing measurement for the standard luminosity ($\mathscr{L} = 10^{33}$ cm^{-2} s^{-1}). See Fig. 10 for details.

Table 2
Sampling patterns studied. The period of the sampling is 16 ns, the beam crossing period at the SSC. The common sample in the center of patterns, A, B, and C is placed near the peak of the waveform with $t_m = 50$ ns. Pattern D, which has samples over the full waveform, contains 44 samples for $t_m = 50$ ns

Pattern name	Sampling pattern
A	0000111110000
B	0010101010100
C	1001001001001
D	···1111111111111···

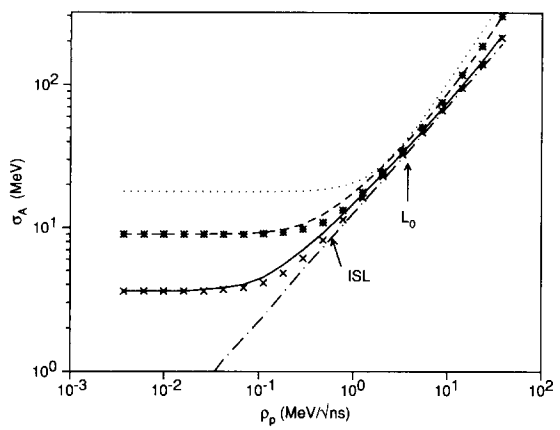

Fig. 12. Amplitude resolution using the method of optimal filtering versus the pileup noise density $\rho_p = \sigma_p / \sqrt{S_p}$. The dot-dash curve is the ISL formula, and the solid and dashed curves are from the finite sampling integral. The dotted curve is the value of σ_s for a single sample. The symbols are values of σ_A found from the numerical solution in the time domain. The full sampling solution (solid curve and (×) symbols), described in the text, sets a lower limit to the value of σ_A which can be achieved with a finite number of samples. The solution with 5 samples (pattern B) is the dashed curve and asterisk (*) symbols. The vertical arrow marks the value at which the luminosity is 10^{33} cm^{-2} s^{-1}, corresponding to the standard case used in this paper.

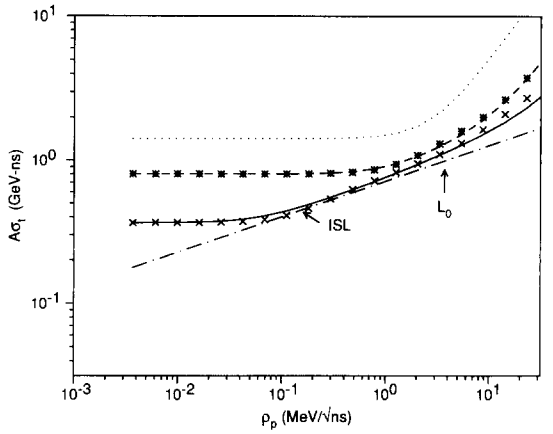

Fig. 13. Time resolution using the method of optimal filtering plotted versus the pileup noise density $\rho_p = \sigma_p / \sqrt{S_p}$. The dot-dash curve is the ISL formula, and the solid and dashed curves are from the finite sampling integral. The dotted curve is the value of $A\sigma_\tau$ that would be obtained using an ideal constant fraction discriminator working at the point of steepest slope in the waveform. The symbols are values of $A\sigma_\tau$ found from the numerical solution in the time domain. The full sampling solution (solid curve and (×) symbols), described in the text, sets a lower limit to the value of $A\sigma_\tau$ which can be achieved with a finite number of samples. The solution with 5 samples (pattern B) is the dashed curve and asterisk (*) symbols. The vertical arrow marks the value at which the luminosity is 10^{33} cm^{-2} s^{-1}, corresponding to the standard case used in this paper.

leads to a wider integral limits, which reduces the errors on the parameters, as is shown in Figs. 12 and 13. For the cases with 5 samples, one sees a general correspondence between the sample spacing and the frequency limits, but pattern B gives generally better performance in the amplitude measurement. This behavior is intimately related to the form of the composite weighting and response functions, whose complexities preclude a simple intuitive explanation.

To illustrate the behavior of the optimal filter solutions as a function of luminosity, we solve for σ_A and $A\sigma_\tau$ for fixed values of ρ_t and t_d. In Fig. 12 we

Table 3
Parameters for the four sampling patterns discussed in the text. T is the effective measurement time, W is the effective width of the response function, and m_p and m_t are the effective slopes in the pileup and thermal noise limits, respectively

Pattern	T [ns]	W [ns]	m_t [ns]$^{-1}$	m_p [ns]$^{-1}$	$\omega_{A,l}$ [10^6 rad/s]	$\omega_{A,u}$ [10^6 rad/s]	$\omega_{\tau,l}$ [10^6 rad/s]	$\omega_{\tau,u}$ [10^6 rad/s]
A	79.1	62.4	0.0111	0.0558	9.44	59.9	15.9	77.8
B	65.4	46.1	0.0127	0.0282	11.4	68.1	18.0	51.5
C	79.9	65.9	0.0119	0.0535	9.34	47.7	13.9	68.9
D	146.0	27.1	0.0098	0.0854	5.10	115.9	4.03	134.6

compare the values given by the FSI in our standard case, for two sampling patterns: one with 5 samples (pattern B) and one with full sampling (pattern D). We show both the time-domain calculations as well as the values found from FSI, and the agreement is good. Essentially, one determines the values of $\omega_{A,l}$ and $\omega_{A,u}$ using time domain calculations for the two limiting cases, and the FSI is used to interpolate all intermediate values. In Fig. 13, we show the time domain calculation and FSI calculation for the same cases given in Fig. 12. Again, it is seen that FSI is a reasonably good representation of the time-domain calculations.

From the discussion of section 4.6, there are three regions of interest: (1) the region where thermal noise dominates, (2) the region where both thermal and pileup noise are important, and (3) the region where pileup noise dominates. Each of the regions has a characteristic dependence on ρ_t or ρ_p, which is evident from Eqs. (82) and (83) and can be seen in Figs. 12 and 13. The plots also illustrate how the pattern with 5 samples compares with the results of full sampling and also how they compare with a single measurement at the peak of the waveform in the case of the amplitude or with an ideal constant fraction discriminator in the case of the timing measurement. The abscissa in the plot is the pileup noise density, but in a more general sense, the plot shows the behavior of the system as a function of (1) luminosity ($\rho_p \propto \mathscr{L}^{1/2}$), with luminosity increasing to the right, (2) depth in the calorimeter, increasing to the left, and (3) area of the tower size, increasing to the right ($\rho_p \propto \mathscr{A}^{0.76}$, while $\rho_t \propto \mathscr{A}^{0.5}$).

In Fig. 14 we show a plot of the width of the amplitude response function as a function of ρ_p for sample patterns B and D, effective width in the along with the effective width in the infinite sampling limit. Note that the width of the response function for the practical case of 5 samples more or less approximates the ISL formula in the central region but there are very large differences in either the pileup or thermal noise regions. This is easy to understand: in the thermal noise region, the filter would like to produce a response function with a large width, but it is limited by the finite sampling interval, whereas in the pileup noise region, where a narrow width is desired, it is limited by the size of the sampling period. Note that the full sampling solution is able to approximate much closer the ISL width, but it eventually is limited to finite values for the same reasons.

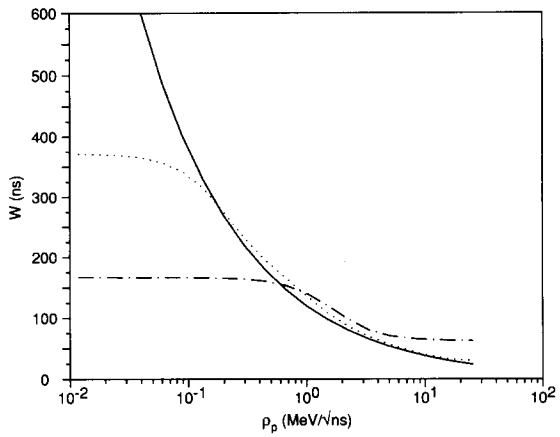

Fig. 14. Effective width of the amplitude response function, plotted against the pileup noise density $\rho_p = \sigma_p / \sqrt{S_p}$. The solid curve is the ISL formula, while the dotted curve is obtained from the time-domain optimal filter calculation, assuming samples taken over the entire waveform (pattern D). The failure of the full sampling curve to follow the ISL curve is a consequence of the finite sampling interval and the minimum time between samples. The dot-dash curve is obtained with the 5-sample sampling pattern (pattern B). This quantity determines the contribution of pileup noise to the value of σ_A.

5. Data acquisition considerations

In designing the data acquisition and triggering systems for a large calorimeter, it is important to understand the implication of various design choices at the analysis stage. The choice of the number of samples and where they are placed with respect to the origin of the signal is an obvious example. Because of the high channel count, data volumes will necessarily be quite large, so it is useful to reduce the number of samples to the minimum, consistent with the goals of the desired amplitude and timing precision. Another important design choice is the type of pre-filter used in the electronics chain and its associated time constants. Practical considerations restrict the peaking times to ≈ 20 ns or greater, but considerable effort is required to build a system with high analog bandwidth, so it is important to understand the implications of bandwidth limiting in the front end electronics. Finally, the question of the precision required for the digitization stage is one that has implications for the precision of the analyzed data, and how the digitization error propagates to the error in the final result depends on choices for both the shaping time and the number of samples. These questions are addressed under the assumption that the data are processed using the method of optimal filtering.

5.1. Choice of the pre-filter shaping time

In sections 4.6 and 4.7 we have seen that the use of optimal filtering bestows upon the system a certain insensitivity to the pre-filter shaping time t_m. But there are limits to the degree to which the optimal filter can

compensate for an inappropriate choice of the shaping time, and it is therefore useful to examine a method for choosing t_m.

We consider the case for a calorimeter cell operating at a given luminosity, i.e. with ρ_p and ρ_t fixed. An intuitive choice for t_m would be that value which minimizes σ_s^2, the variance of the signal including both pileup and thermal noise. This value can be easily found. The expression for σ_s^2 is

$$\sigma_s^2 = \sigma_t^2 + \sigma_p^2 = \rho_p^2 S_p(t_m) + \rho_t^2 \frac{I_1(t_m)}{r_q^2(t_m)},$$

in which S_p is defined in Eq. (17), I_1 in Eq. (17), and r_q in Eq. (5). To a good approximation, the functional dependencies of these quantities on t_m is given by $I_1 = a_1/t_m$, $S_p = a_p t_m$, and $r_q = t_m/t_d$, in which a_1 and a_p are dimensionless constants of order unity. This results in a simple expression for σ_s as a function of t_m which has a minimum at

$$t_m^0 = \left(\frac{3a_1}{a_p}\right)^{1/4} \sqrt{\frac{\rho_t t_d}{\rho_p}}, \tag{84}$$

at which point the values for the components of σ_s^2 are:

$$\sigma_p^2 = 3^{1/4}\left(a_1 a_p^3\right)^{1/4} \sqrt{\rho_t t_d \rho_p^3},$$

$$\sigma_t^2 = 3^{-3/4}\left(a_1 a_p^3\right)^{1/4} \sqrt{\rho_t t_d \rho_p^3},$$

which yields

$$\sigma_s^2 = 4\left(\frac{a_1 a_p^3}{27}\right)^{1/4} \sqrt{\rho_t t_d \rho_p^3}. \tag{85}$$

Note that at the optimal shaping time

$$\sigma_p = \sqrt{3}\,\sigma_t.$$

There is an interesting similarity between this expression and that for $\tilde{\sigma}_A^2$ (Eq. (71)), the optimal filter result in the infinite sampling limit. This argument also gives the value 3 found in Eq. (74) for the ratio of the pileup to thermal contribution to the variance. The numerical coefficient appearing in Eq. (84), $(3a_1/a_p)^{1/4}$, is reasonably insensitive to the choice of t_m or to n, the order of integration of the filter. For the values shown in Table 1, we find that this factor is within 5% of the value 1.5. Thus, to this level of accuracy, the expression for the optimal measurement time becomes

$$t_m^0 \approx 1.5\sqrt{\rho_t t_d/\rho_p}.$$

For our standard case of an $(RC)^2-(CR)^2$ filter, we find a value of 4.06 for the numerical coefficient in Eq. (85). Comparing this with the factor of $\sqrt{8}$ in Eq. (71) we see that the optimal filter in the ISL yields a lower value of the variance than σ_s^2:

$$\tilde{\sigma}_A^2 = 0.69\sigma_s^2.$$

Another approach to the question of optimal shaping time is to examine the behavior of the optimal filter itself as a function of t_m. We consider the contribution of the pileup and thermal noise to the value of σ_A^2 as a function of t_m. From Eq. (48), noting that $\xi_t \propto \sigma_t^2$ and $\xi_p \propto \sigma_p^2$, we can write

$$\sigma_A^2 = \xi_t + \xi_p = D_t\sigma_t^2 + D_p\sigma_p^2, \tag{86}$$

in which the noise factors D_t and D_p are dimensionless numbers (D_p and D_t can be expressed in terms of T and W, but that is unnecessary for this argument). They are the factors by which the thermal noise and pileup noise are weighted by the optimal filter. From Eq. (72) we see that, in the ISL, $\tilde{\xi}_t$ and $\tilde{\xi}_p$ are both constants, independent of the measurement time. Thus we infer that the measurement time dependencies of D_t and D_p are the inverse of those of σ_t^2 and σ_p^2, respectively. We suggest that a useful criterion for the pre-filter shaping time would be that value for which $D_p = D_t$, i.e. that at the optimal value for the measurement time, it is not necessary for the filter to weigh the two sources of noise unequally. From Eq. (74) we see that

$$\frac{\tilde{\xi}_p}{\tilde{\xi}_t} = \frac{D_p\sigma_p^2}{D_t\sigma_t^2} = 3.$$

When $D_t = D_p$, the $\sigma_p^2 = 3\sigma_t^3$ and

$$\rho_p a_2 t_m^{opt} = \frac{3a_1\rho_t}{\left(t_m^{opt}\right)^3},$$

giving

$$t_m^{opt} = \left(\frac{3a_1}{a_p}\right)^{1/4} \sqrt{\frac{\rho_t t_d}{\rho_p}} = t_m^0, \tag{87}$$

showing that both criteria yield the same result in this approximation.

In Fig. 15 we illustrate the equivalence of the two methods. While the variation of σ_s^2 with respect to t_m shows a minimum at t_m^0, it is quite shallow, due to the extreme asymmetry of the curve about the minimum. The crossing point of the D_t and D_p curves is a much more sharply defined point. Note that the values of the coefficients at which they cross is about 0.73, from which one can conclude that at $t_m = t_m^{opt}$,

$$\sigma_A^2 = D_t\sigma_t^2 + D_p\sigma_p^2 \approx 0.73\sigma_s^2$$

which is slightly larger than the value found from the criterion based on $\tilde{\sigma}_A$, as expected. This argument also indicates how to choose the value of t_m to achieve optimum timing performance. Since $\zeta_p/\zeta_t = 1/3$, this optimum occurs where $3\sigma_p^2 = \sigma_t^2$, giving $t_m^{opt}(\text{timing}) = t_m^{opt}(\text{amplitude})/\sqrt{3}$.

5.2. Quantization accuracy

We now turn to the question of how the quantization accuracy of the digitization of the samples S_i

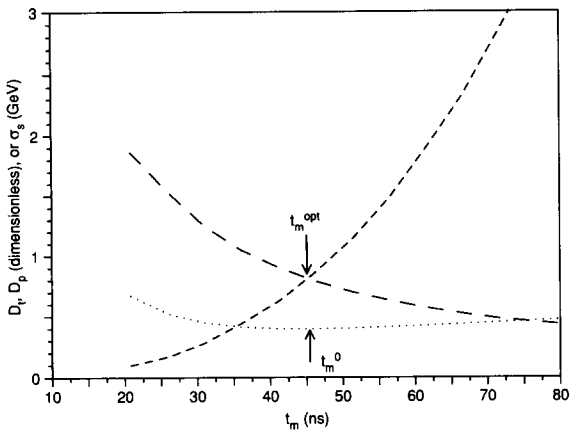

Fig. 15. Graph showing the equivalence between the two methods for determining the optimum pre-filter shaping time. The dotted curve is the value of σ_S as a function of t_m, where it is seen that there is a very shallow minimum at t_m^0. The two dashed curves are the noise factors D_p(falling) and D_t(rising), which are the weights given the pileup and thermal variances for the amplitude in the optimal filtering method ($\sigma_A^2 = D_p\sigma_p^2 + D_t\sigma_t^2$). The point t_m^{opt} occurs where the two noise factors are equal. The data are for the standard case of a 0.04×0.04 EM cell.

affects the variance of the parameters. Intuitively one suspects that if there are large negative values of the filter coefficients, which indicates that the final value of the parameter is the difference of two large numbers, there may be increased sensitivity to the quantization error. It is easy to show that this is in fact the case. If we assume that a linear ADC scale is used, with a maximum range of $\Delta E = E_{max} - E_{min}$, then for a precision of n_b bits, the quantization error in S_i is

$$\sigma_q = \Delta E/\sqrt{12}N, \tag{88}$$

in which $N = 2^{n_b} - 1$ is the full range of the ADC.

The amplitude A and the time shift τ are related to the samples S_i by the simple linear expressions

$$A = \sum_i a_i S_i,$$

$$\tau = \frac{1}{A}\sum_i b_i S_i.$$

The propagation of the quantization error to the fitted parameters is straightforward:

$$q_A = \sigma_q\sqrt{\sum a_i^2} = \sigma_q R_A, \tag{89}$$

$$Aq_\tau = \sigma_q\sqrt{\sum b_i^2} = \sigma_q R_\tau, \tag{90}$$

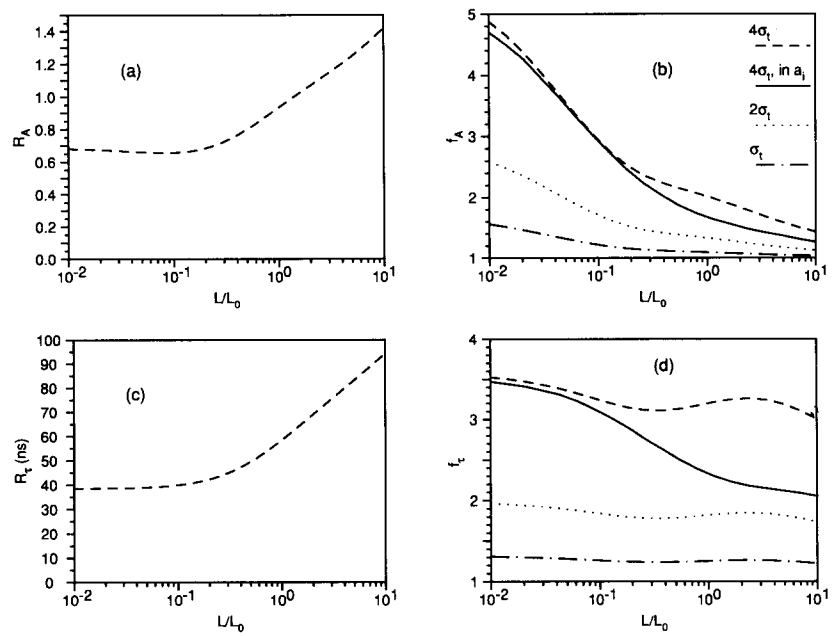

Fig. 16. Values of the quantization coefficients and their effect on the values of σ_A and $A\sigma_\tau$ for the case of 5 samples (pattern B), as a function of relative luminosity ($\mathscr{L}_0 = 10^{33}$ cm^{-2}s^{-1}). (a) Value of $R_A = q_A/\sigma_q$. (b) Factor f_A by which the value of σ_A is increased by the effect of quantization error for the standard case. The values of σ_q, chosen to be multiples of the thermal noise σ_t, are indicated in the legend. The solid curve indicates the effect of including the quantization error in the calculation of the coefficients, as discussed in the text. (c) Value of $R_\tau = Aq_\tau/\sigma_q$. (d) Factor f_τ by which the value of $A\sigma_\tau$ is increased by the quantization error, as explained in (b). The legend for (b) also applies to (d).

in which q_A and Aq_τ are the contributions of the quantization error to the variances of A and $A\tau$, respectively and must be added in quadrature to σ_A and $A\sigma_\tau$. The quantities R_A and R_τ, being the factors which determine how the sample quantization error propagates to the quantization errors in A and τ, characterize a particular solution for the coefficients. These quantities increase with increasing luminosity, as can be seen in Fig. 16, and this is understood as a consequence of the appearance of negative coefficients which are needed to reduce the effective widths of the response functions. If the quantization error becomes a significant component of the noise terms, it is possible to reduce its effect through the inclusion of this term in Eq. (32) in calculating the coefficients. The term R_{ij} is incremented by the amount $\delta_{ij}\sigma_q^2$, and coefficients found are those which minimize the variance including the effects of quantization error. In Figs. 16b and 16d we show the factors f_A and f_τ by which the values of σ_A and $A\sigma_\tau$ are increased by the effects of quantization errors. The factors are defined as

$$f_A = \sqrt{1 + \frac{q_A^2}{\sigma_A^2}} ,$$

and

$$f_\tau = \sqrt{1 + \frac{q_\tau^2}{\sigma_\tau^2}} .$$

We show results for three values of σ_q, where the quantization error is ignored in the calculation of the coefficients. For the largest quantization error studied ($\sigma_q = 4\sigma_t$) we show for comparison the effect of including it in the solution. It can be an important effect when the pileup noise is large.

It should also be mentioned that in some data acquisition systems, the use of a dual-range ADC may be employed, with a break point at a certain value of the pulse height. When a pulse whose peak is just above the break point is measured, samples near the peak may be digitized on the low-gain scale, whereas samples further from the peak are digitized on the high-gain scale with lower quantization error. By calculating coefficients in which the individual quantization errors are introduced in the minimization process, it is possible to weigh the samples individually to correctly account for their precision.

For the case where a logarithmic scale is used, the quantization error in a sample S is given by

$$\sigma_q^{\log} = \frac{(f-1)}{\sqrt{12}}(S - E_{\min}),$$

in which

$$f = \left(\frac{\Delta E}{E_0}\right)^{1/N}$$

and E_0 represents the units of E. Propagating this error to the error in the parameters yields the following expressions

$$q_A^{\log} = A\frac{f-1}{\sqrt{12}}\left(\sum a_i^2 g_i^2 - \frac{2E_{\min}}{A} \times \sum a_i^2 g_i + \frac{E_{\min}^2}{A^2}\sum a_i^2\right)^{1/2},$$

$$q_\tau^{\log} = \frac{f-1}{\sqrt{12}}\left(\sum b_i^2 g_i^2 - \frac{2E_{\min}}{A} \times \sum b_i^2 g_i + \frac{E_{\min}^2}{A^2}\sum b_i^2\right)^{1/2}.$$

Note that for the case $E_{\min} = 0$, $q_A^{\log}/A$ and $q_\tau^{\log}$ are independent of the signal amplitude. The quantities $\Sigma a_i^2 g_i^2$ and $\Sigma b_i^2 g_i^2$ are smaller than R_A and R_τ, respectively, since $g_i \le 1$.

Use of the logarithmic scale is advantageous in situations where the fractional energy resolution is constant, since the quantization error then remains the same proportion of the resolution over the entire energy scale. For a calorimeter whose resolution $\sigma_E \propto \sqrt{E}$, the fraction of error due to quantization increases with E when a logarithmic scale is used and decreases with E when a linear scale is used.

5.3. Number and position of the samples

The choice of the number and position of the samples can be driven by a number of criteria, which sometimes conflict. We itemize here a few observations we have made in investigating a variety of sampling patterns.

– A finite set of samples may be chosen with the goal of achieving optimal amplitude or timing resolution. These are generally complementary sets, if the number of samples is limited to 3 or less. Thus, in order to use a common set of samples to determine both amplitude and timing, one achieves noise values within about 20% of the ISL values with at least five samples.

– For a given number of samples (≥ 5) in the ISL region, the sensitivity to the positioning of the samples is quite low. However, if the system operates in either the thermal noise or the pileup noise regions, there is a stronger dependence on certain features of the sampling pattern. In the thermal noise region, better resolution is obtained by spacing the samples widely, in order to increase the width of the effective weighting function. However, when the separation between the samples becomes sufficiently wide, significant ripples can appear in the weighting function (see Fig. 8), which can increase the thermal noise.

Table 4
Values of the errors on the parameters A and τ obtained for the 4 sampling patterns discussed in section 4.6 for three different values of luminosity. The quantization coefficients R_A and R_τ are also given in each case. The effect of quantization error was not included in the calculation of the coefficients

Luminosity [$cm^{-2}s^{-1}$]	Pattern	σ_A [MeV]	$A\sigma_\tau$ [GeV ns]	R_A	R_τ [ns]
10^{30}	A	12.0	0.94	0.64	53
	B	9.1	0.80	0.60	39
	C	9.0	0.75	0.86	42
	D	4.2	0.42	0.64	59
10^{33}	A	41.1	1.50	0.95	49
	B	38.2	1.37	0.93	58
	C	40.6	1.28	0.98	50
	D	35.7	1.15	0.84	51
10^{34}	A	107.3	3.70	3.79	67
	B	99.0	2.38	1.42	94
	C	111.1	2.39	1.33	62
	D	83.1	1.92	3.28	129

– Quantization error can be affected by the sampling pattern, and for the low luminosity case can generally be reduced by using closely spaced samples. At high luminosity, where the optimal filter reduces the effective width of the amplitude response function by introducing large coefficients of opposite signs, sampling patterns with closely spaced samples result in large quantization coefficients.

As an example of the effects of choosing different sampling patterns on the resulting errors in A and τ, we give in Table 4 the results obtained for the four sampling patterns introduced in section 4.6 at three different luminosities. It is seen that the sensitivity to the pattern is largest for high luminosity, and for the particular case studied, pattern B is somewhat better than patterns A and C. It is interesting that near the luminosity where $t_m = t_m^0(0.5 \times 10^{33}\ cm^{-2}s^{-1})$, all of the patterns (including full sampling) are nearly equivalent, as can also be concluded from Figs. 12 and 13. At low luminosity, it is clear that the choice of sampling pattern can be very important.

The shaping time of the pre-filter circuit depends on the values of components such as resistors and capacitors as well as distributed inductances and capacitances of connections and circuit routes. Since these may differ from channel to channel, it is important to investigate the sensitivity of the resolution of the system to the actual value of shaping time t_m for the case where the sampling pattern is held fixed. In Fig. 17 we show the variation of σ_A and $A\sigma_\tau$ for the four different sampling patterns versus the pre-filter shaping time. The coefficients a_i and b_i are recalculated for each value of t_m, corresponding to the case where the shaping time is known. The main effect here is that the samples are being held fixed in time while the shaping time is varied. Thus a different value of t_m corresponds to sampling a different part of the waveform, in the case of the three patterns with 5 samples. Since the entire waveform is sampled for all t_m for pattern D, there is very little sensitivity to t_m except at the lowest values, where the effect of limited spacing between the samples ($T_c = 16$ ns) becomes evident.

6. Monte Carlo tests

In order to verify some of the results obtained in this paper, we have written a Monte Carlo program to simulate the addition of the thermal and pileup noise to a shaped signal of known amplitude, and then to reconstruct the amplitude using the optimal filtering method. One of the main motivations for carrying out this study is to ascertain the extent to which the non-Gaussian nature of the pileup distribution compromises the approach of treating it as essentially a Gaussian distribution.

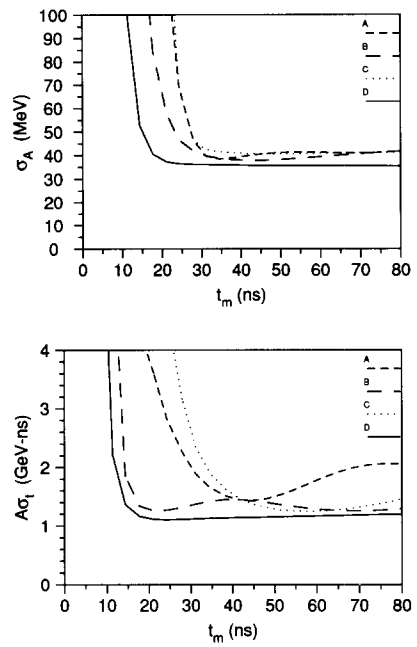

Fig. 17. Variation of σ_A and $A\sigma_\tau$ as a function of measurement time t_m for the four different sampling patterns (A, B, C, and D) described in the text. The positions of the samples are held fixed in time, so different parts of the waveform are sampled as the shaping time is varied. The coefficients are recalculated for each value of t_m. The patterns with 5 samples (A, B, and C) have the central sample placed near the peak for the case $t_m = 50$ ns.

6.1. Procedure

The model for thermal noise approximates the actual noise generation process by an amplitude distribution of a Gaussian shape with a width ρ_t and multiplying this amplitude by $h'(t)$. The interval chosen for the origination of the waveforms is the period of the machine clock (16 ns). This distribution is clearly incorrect, since noise pulses are generated uniformly in time, and therefore exhibit additional fluctuations due to the Poisson process. In fact, generating noise signals in this way produces a variance described by Eq. (17) rather than the correct variance given by Eqs. (11) and (12). In order to simulate the Poisson nature of the fluctuations, we define an elementary noise signal as one with a Gaussian amplitude distribution. For each beam crossing we obtain the number N of such signals occurring, according to a Poisson distribution of mean frequency $1/T_c$. We then sum N samples from the Gaussian distribution to find the amplitude of the series thermal signal for the crossing. The derivative of the impulse response $h'(t)$ is then multiplied by this amplitude, and the waveform is propagated to the succeeding crossing, where the process is repeated. This procedure is found to give an adequate representation of the series thermal noise fluctuations, as is seen in our results presented below.

The model for the pileup noise is somewhat more problematical and, as mentioned above, is one of the primary motivations for this study. The procedure for calculating the distribution of energy deposition in a calorimeter cell is discussed in section 3.2.3, and the resulting histogram for one cell is shown in Fig. 18. Note that a large fraction of the histogram is in the lowest bin, i.e. with zero energy deposition. This is simply the result of particles missing the cell (or cells in its immediate neighborhood) a substantial fraction of the time. The remainder of the distribution shows a falloff characteristic of the exponential distribution of the inclusive cross section, as is evident from the histogram. As is discussed in section 3.2.3 we characterize this distribution with its variance and proceed to treat the derived quantity σ_p when for example combining it with σ_t (see Eq. (44)) as if it were a Gaussian-distributed quantity. We wish to test the degree to which we can rely upon the central limit theorem for this procedure.

We proceed by working with two distributions for the pileup noise: $f_{NG}(E)$, which is the obviously non-Gaussian histogram of Fig. 18 and a Gaussian distribution $f_G(E)$, defined as

$$f_G(E) = \frac{1}{\sqrt{2\pi}\,\rho_p} e^{(E-\langle E\rangle)^2/2\rho_p^2}$$

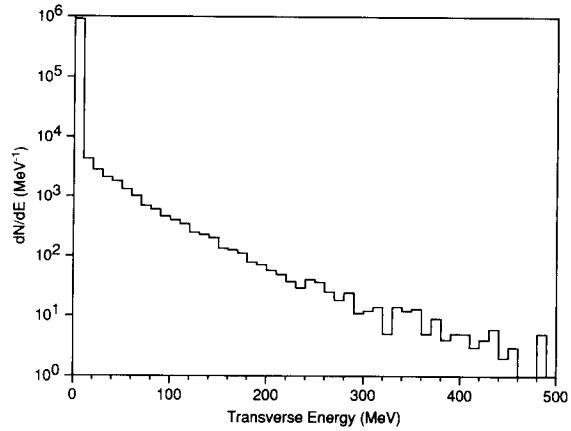

Fig. 18. Histogram of the transverse energy deposited per crossing in an EM cell of size 0.04×0.04 at a luminosity of 10^{33} cm^{-2}s^{-1}. The events are 2-jet events, with the p_T of one of the jets between 5 and 10 GeV/c, as produced by the ISAJET event generator. The large spike in the first bin is caused by the low occupancy. The exponential tail is characteristic of the E_T distribution of the particles.

in which $\langle E\rangle$ is the mean value of $f_{NG}(E)$ and ρ_p^2 is its variance. In either case E represents the pileup energy seen in a calorimeter cell for one machine crossing, where the number of interactions is assumed to be Poisson distributed with a mean of 1.6 events. (This number comes from the assumption of a total cross section of 100 mb, a machine luminosity of $\mathscr{L} = 10^{33}$ cm^{-2}s^{-1} and a machine clock period of 16 ns.) The random variable E is then multiplied by the signal waveform $g(t)$, and we proceed to the next crossing.

At any crossing the total noise signal $n(t)$ is found by adding together the thermal and pileup signals from all previous crossings occurring within the deviation of the signal waveform $g(t)$. We calculate $\sigma_s^{mc} = \sqrt{\mathrm{Var}(n)}$ for comparison with the expected value σ_s^2 from Eq. (44).

At a specific crossing, after the stationary value of $n(t)$ is reached (i.e. after the duration of the signal $g(t)$), a signal waveform of a given energy E_0 is simulated by generating a waveform $U(t) = E_0 g(t)$. To this signal is added the noise signal $n(t)$ at each crossing. For the reconstruction phase, a mask is used to pick those crossings that are to be sampled. We give results of the pattern discussed in section 5.3 with 5 samples (pattern B), since it is representative of the type of data that might be available in an offline analysis. The values of the 5 samples $S_j^k = U_j + n_j^k$, in which j is the crossing index and k is the event index, are then stored in a data array. The optimal filter coefficients, calculated according to the prescription discussed in section

4.2 are then used to find the noise-distorted values of the amplitude and timing parameters for the kth event:

$$A_k = \sum_i a_i S_i^k,$$

$$A_k \tau_k = \sum_i b_i S_i^k.$$

After processing a number N of events we find the variances Var(A) and Var($A\tau$) are calculated. The identical procedure is carried out for both pileup distributions $f_{NG}(E)$ and $f_G(E)$.

6.2. Results of the simulation

We begin by showing the amplitude distribution of the baseline obtained for the non-Gaussian distribution of the pileup noise. In Fig. 19a we show how the distribution of Fig. 18 is transformed by the introduction of both bipolar shaping and smearing in time. While the distribution is still quite asymmetric, it now has zero mean (guaranteed by the area balance of the pre-filter shaping function) but with a shape which is still quite non-Gaussian. We superpose on the histogram a Gaussian of the width $\sigma_{hist} = 33$ MeV, which is the square root of the variance of the histogram. In Fig. 19b, we show how the distribution is altered when thermal noise is added, and again superpose a Gaussian of width 42 MeV, given by the histogram. We now compare the variance of Fig. 19a with the expected value, given by Eq. (17). The value of the pileup noise

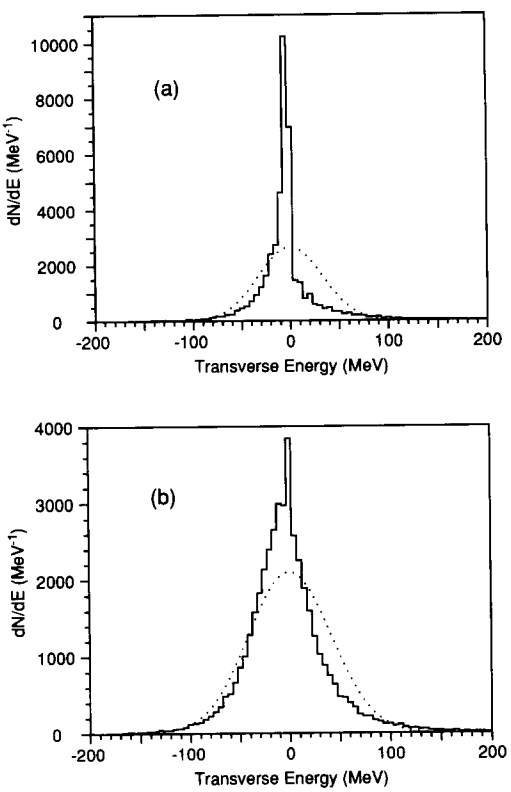

Fig. 19. (a) Distribution of the baseline found after simulating the effect of bipolar shaping and the time distribution for the data of Fig. 18. The dotted curve is a Gaussian of the same area and variance as the histogram. (b) Data of (a) but with series thermal noise added to the pileup noise. As in (a), the dotted curve is a Gaussian of the same area and variance as the histogram.

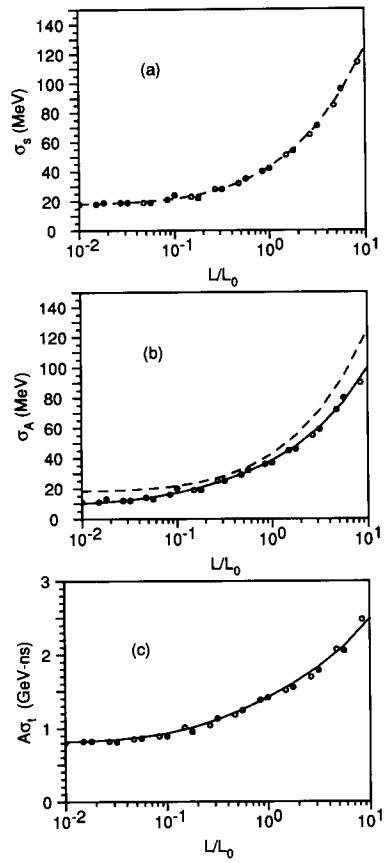

Fig. 20. (a) Monte Carlo data for the value of σ_s^{mc} as a function of luminosity. The closed circles are data taken from the non-Gaussian distribution (i.e., the data of Fig. 18) and the open circles are for data taken from a Gaussian distribution with the same variance. The dashed curve is calculated from the formula $\sigma_s^2 = \sigma_t^2 + (\mathscr{L}/\mathscr{L}_0)\sigma_{p0}^2$, in which σ_{p0}^2 is the pileup variance calculated for $\mathscr{L} = \mathscr{L}_0$. Statistical errors are smaller than the size of the symbols. (b) Corresponding value of σ_A^{mc}. The dashed curve is the same curve for σ_s shown in (a) and the solid curve is the expected value for σ_A from the optimal filter method, assuming 5 samples (pattern B). (c) Corresponding value of $A\sigma_\tau^{mc}$. The curve is the expected value for $A\sigma_\tau$ from the optimal filter method, assuming 5 samples. Statistical errors are smaller than the size of the symbols.

density from the histogram of Fig. 18 is $\rho_p = 3.7$ MeV/$\sqrt{\text{ns}}$. From Table 1 we find that $S_p = 104$ ns for our standard case of $(RC)^2 - (CR)^2$ pre-filter shaping with $t_m = 50$ ns and $t_d = 400$ ns. This yields

$$\sigma_p = \rho_p \sqrt{S_p / T_c} = 38 \text{ MeV},$$

at $\mathscr{L} = \mathscr{L}_0$, in reasonable agreement with the value of σ_{hist} found above. The $\sim 20\%$ difference between the two values is presumably the effect of the non-Gaussian nature of the distribution shown in Fig. 18.

The remainder of the study is to carry out the procedure outlined above, finding Monte Carlo values for $\sigma_s^{mc} = \sqrt{\text{Var}(n)}$, $\sigma_A^{mc} = \sqrt{\text{Var}(A)}$, and $A\sigma_\tau^{mc} = \sqrt{\text{Var}(A\tau)}$. We choose to display these quantities as a function of luminosity, passing from the region where $\sigma_t \gg \sigma_p$ to the region where $\sigma_t \ll \sigma_p$. If there were an important effect due to the non-Gaussian nature of the pileup noise, one would expect to see a difference between the two data sets at high luminosity. No such effect is seen at the level of statistical accuracy of these simulations, which is approximately 1%.

7. Summary and conclusions

The main point of this work has been to show the utility of measuring multiple samples on a shaped waveform and combining them to find values of the unknown parameters A and $A\tau$. The principal conclusion is that when the value of the pre-filter shaping time is chosen to give the minimum value for a particular level of pileup and thermal noise, the error in A found from measuring one sample at the peak is very close (typically within 20%) of that which can be achieved by measuring any number of samples on the waveform. The main advantage in multiple sampling comes in cases where the shaping time is not the optimal one. The optimum filter method, in effect, redefines the shaping time numerically and therefore permits one to come close to optimal value for the error even though one may be rather far from the optimal shaping time for the pre-filter.

There are limits to how well the method can work, which become more restrictive as the number of samples is decreased. The precision of the measurement can be seriously compromised if the pre-filter shaping time t_m is significantly longer than the optimal value, as the quantization error may become quite significant. This occurs since the digital filtering method effectively creates the difference between large numbers in coming to its solution, as is discussed in section 5.2.

Several references are made to the "ISL" or "infinite sampling limit" throughout the text. These are analytic expressions found using the frequency domain formalism, and they can be visualized as the values (for σ_A and $A\sigma_\tau$) which would be obtained if one could take infinitely many samples over the entire waveform. These expressions are useful both because they represent limits which can be approached in any practical situation and also because in many cases of practical interest, where both pileup and thermal noise are present, they approximate the practical solution to within about 20%. Quantities calculated in this limit are designated by a tilde ($\sim$). A more refined version of the frequency domain solution, which we call finite sampling occurs when we evaluate the frequency integrals with finite limits. An interesting limit is the case of full sampling, in which samples are taken over the entire waveform at the beam crossing period T_c. This solution has the property (unlike the ISL solution) that it gives meaningful values in the limit where either the pileup or thermal noise vanishes. It is also useful as a lower limit to the values of σ_A and $A\sigma_\tau$ which can be obtained with a practical number of samples. These quantities include the effects of the restriction of period of the samples to T_c but still do not represent a practical situation, since samples are taken over by the complete waveform. They do have the advantage, however, that they represent properly the values in the limit where the pileup or thermal noise dominate the errors in the samples. In order to understand the effect of choosing a small number of samples, we make frequent comparisons numerically to the full sampling limit.

In order to demonstrate the utility of the ISL formulae, we compare in Table 5 the quantities calculated in three ways for our sample case, where the luminosity is 10^{33} cm^{-2} s^{-1}. The accuracy of the ISL formulae

Table 5
Comparison of results for the noise in the amplitude and timing measurement at the standard luminosity (10^{33} cm^{-2} s^{-1}) under different sampling conditions. The ISL formulae and results are shown, along with the values obtained with full sampling (sampling pattern D) and with 5 samples (pattern B). The effective width W measures the sensitivity to pileup noise, and the effective slope m indicates the sensitivity of the timing measurement

Quantity	ISL formula	ISL	Pattern D	Pattern B
σ_A [MeV]	$(8\rho_t t_d \rho_p^3)^{1/4}$	34.0	36.8	38.1
$A\sigma_\tau$ [GeV ns]	$(8\rho_t^3 t_d^3 \rho_p)^{1/4}$	1.00	1.14	1.40
W [ns]	$\frac{3\sqrt{2}}{2}\left(\frac{\rho_t t_d}{\rho_p}\right)^{1/2}$	62	69	76
m [ns^{-1}]	$\frac{3\sqrt{2}}{2}\left(\frac{\rho_p}{\rho_t t_d}\right)^{1/2}$	0.034	0.031	0.028

becomes poor whenever the thermal noise or pileup noise dominates, as discussed in section 4.6.

One of the useful applications of the ISL formulae is in their application to situations in which the noise in the calorimeter as a function of luminosity $\mathscr{L}$, area $\mathscr{A}$ in the calorimeter is needed. As pointed out in section 3.2.3, the pileup noise density can be expressed as a function of these three variables by the simple equation

$$\rho_p = 380(\Delta\eta\Delta\phi)^{0.76}\left(\frac{\mathscr{L}}{\mathscr{L}_0}\right)^{1/2} \text{ MeV}/\sqrt{\text{ns}}\,.$$

The thermal noise density, from Eqs. (11) and (12), is

$$\rho_t = \frac{1}{\sqrt{2}}\frac{e_n C_{tot} W_{ion} a_e}{\eta_s q_e}\,.$$

By expressing ρ_t in terms of the geometrical constants which determine the capacitance C and the sampling fraction η_s, one can obtain scaling laws for $\tilde{\sigma}_A$, and $A\tilde{\sigma}_\tau$.

The optimal pre-filter shaping time may be found using two different criteria, which give very similar results. One criterion simply requires that $\sigma_s = \sqrt{\sigma_t^2 + \sigma_p^2}$ is a minimum; the other requires that the optimal filter weighs the thermal and pileup noise equally. In either case the value for the optimal shaping time is given approximately by:

$$t_m^0 \approx 1.5\sqrt{\rho_t t_d/\rho_p}\,.$$

Propagation of the quantization error to the error in A and τ depends upon the sampling pattern chosen. The coefficients R_A and R_τ characterize the solutions in this regard. Carefully chosen sampling patterns can achieve nearly an additional bit of precision in the amplitude i.e., $R_A \approx 0.6$, but others can produce large values of R_A and R_τ. This is particularly true for cases where pileup noise is important, when the effective width of the amplitude response function becomes shorter than the pre-filter shaping time t_m.

There is no simple answer to the question of how many samples are needed and where should they be placed. As mentioned above, a single sample with $t_m = t_m^0$ yields a value of σ_A which is within 20% of that achieved by full sampling, and therefore the benefits of multiple samples are minimal. Multiple sampling is however useful in cases where:

– pre-filter shaping times are nonuniform from channel to channel due to variation of parameters in the manufacture of integrated circuits;

– it is required to operate the calorimeter over a wide range of machine luminosity;

– non-optimal shaping is used for reasons of convenience, i.e. by installing circuits of similar shaping times in regions of the calorimeter with significantly different values of t_m^0;

– timing information of individual calorimeter cells is important for background rejection.

Depending on which of these criteria dominate the design, different choices for the number and position of the samples may be made. When t_m is not close to t_m^0, it is possible to obtain values of A and τ from optimal filtering with a statistical accuracy significantly better than that of a single sample.

The use of optimal filtering permits a rapid calculation of the parameters with coefficients that can be determined from a knowledge of the thermal and pileup noise in the calorimeter. For this reason it is an algorithm well suited to online applications, as for example in a calorimeter trigger system. The properties of the response functions $y_A(t)$ and $y_\tau(t)$, which can be generated in real time in a digital processor, can be used to establish both the magnitude and timing of the digitized values of the calorimeter signal.

Acknowledgements

It is a pleasure to acknowledge the many useful and enlightening discussions we have had with Veljko Radeka and Sergio Rescia throughout the course of this work. We have also profited from many useful comments from our colleagues in other endeavors involving liquid argon calorimetry, among whom are C. Fabjan, H. Gordon, D. Lissauer, F.E. Paige, and W. Willis. We are indebted to C. de La Taille for bringing to our attention the important role of quantization errors in this analysis. The work was begun under the SSC Generic Detector R&D Program and continued under the R&D program for the GEM experiment. Funding was provided in part by DOE under Contract No. DE-AC02-80ER10667 and Grant No. DE-FG02-90ER40646 at the University of Pittsburgh.

Appendix

Variance of pileup noise for sampled waveforms

Pileup noise is not a true noise source, since it is deterministic, arising from the debris of collisions which are produced by colliding particles. However, in situations where the probability of such interactions is large and the hit occupancy is high enough to create an essentially continuous background, it is convenient, for the reasons shown elsewhere in this paper, to consider it as a noise source. Because of its deterministic nature, this noise source is peculiar in that it occurs at a fixed and known frequency, which distinguishes it from other noise sources. One of the basic theorems relating the variance of the output of system with a know response function due to the frequency of a random

noise source is Campbell's theorem. In this appendix, we derive the analogous theorem, introduced in the main text of the paper as Eq. (17), for the case of a fixed frequency noise source, which for compatibility with current context, is described as a collider producing pileup noise in a calorimeter. However, the theorem itself, which is stated in Eq. (99), is general, the only assumption being that the noise source is stationary and without correlations between pulses.

Consider a single channel in the calorimeter. Number each beam crossing by an index j, which will go from $-\infty$ to $+\infty$. For the beam crossing j, there will be an associated energy (or transverse energy) deposition of E_j. Since each beam crossing is independent of the others, E_j can be considered to be statistically independent of E_k as long as $j \neq k$. The physics determining the energy deposition in each beam crossing is the same, so that $\langle E_j \rangle$ is the same as $\langle E_k \rangle$, and $\langle E_j^2 \rangle = \langle E_k^2 \rangle$.

An energy deposition during beam crossing j, will contribute a signal to subsequent beam crossings which is determined by the signal waveform $g(t)$. If the signal is sampled only at beam crossings, then it can be considered to be a function of the difference in crossing number between the energy deposition and the signal observation. The function $g(t_i - t_j)$ will vanish for values of $t_i - t_j$ outside of a restricted time characterized by the signal waveform. The observed signal in any channel is the sum of the contributions from the preceding crossings. If the signal is sampled only at beam crossings, then

$$S_i = \sum_{j=-\infty}^{+\infty} E_j g(t_i - t_j),$$

where S_i is the observed signal at crossing i, E_j is the energy deposited during crossing j, and $g(t_i - t_j)$ is the signal waveform.

The average value of the observed signal due to pileup in the calorimeter is given by the expectation value of the above expression:

$$\langle S_i \rangle = \left\langle \sum_j E_j g(t_i - t_j) \right\rangle. \tag{91}$$

Since expectation values are linear, and $g(t_i - t_j)$ is just a number, we can bring the expectation values inside the sum, which gives

$$\langle S_i \rangle = \sum_j \langle E_j \rangle g(t_i - t_j). \tag{92}$$

$\langle E_j \rangle$ is independent of j, and $\Sigma g(t_i - t_j)$ extends from $-\infty$ to $+\infty$, so we get

$$\langle S \rangle = \langle E \rangle \sum_{j=-\infty}^{+\infty} g(t_j). \tag{93}$$

To calculate the variance of the signal, we first solve for the value of $\langle S^2 \rangle$.

$$\langle S_i^2 \rangle = \left\langle \left[\sum_{j=-\infty}^{+\infty} E_j g(t_i - t_j) \right] \left[\sum_{k=-\infty}^{+\infty} E_k g(t_i - t_k) \right] \right\rangle \tag{94}$$

$$= \left\langle \sum_{j,k} E_j E_k g(t_i - t_j) g(t_i - t_k) \right\rangle$$

$$= \sum_{j,k} g(t_i - t_j) g(t_i - t_k) \langle E_j E_k \rangle. \tag{95}$$

Two cases can be considered; either $j = k$ or $j \neq k$. In the first case, $\langle E_j E_k \rangle$ yields $\langle E^2 \rangle$. If $j \neq k$, $\langle E_j E_k \rangle$ reduces to $\langle E_j \rangle \langle E_k \rangle$ or $\langle E \rangle^2$ because $j \neq k$ and E_j is independent of E_k. Therefore

$$\langle S_i^2 \rangle = \sum_j g^2(t_i - t_j) \langle E_j^2 \rangle + \sum_{j \neq k} g(t_i - t_j) g(t_i - t_k) \langle E_j \rangle \langle E_k \rangle. \tag{96}$$

The second term can also be expressed as

$$\text{(2nd term)} = \sum_{j,k} (1 - \delta_{jk}) g(t_i - t_j) g(t_i - t_k) \times \langle E_j \rangle \langle E_k \rangle,$$

where δ_{jk} is the Kronecker delta symbol. This can be further expanded to get

$$\text{(2nd term)} = \left[\sum_j g(t_i - t_j) \langle E_j \rangle \right] \times \left[\sum_k g(t_i - t_k) \langle E_k \rangle \right] - \sum_j g^2(t_i - t_j) \langle E_j \rangle^2. \tag{97}$$

The terms enclosed by braces are just $\langle S \rangle$, so substituting into Eq. (96) yields

$$\langle S_i^2 \rangle = \sum_j g^2(t_i - t_j) \langle E_j^2 \rangle + \langle S \rangle^2 - \sum_j g^2(t_i - t_j) \langle E_j \rangle^2. \tag{98}$$

Recognizing that $\langle S^2 \rangle - \langle S \rangle^2$ is just the variance of S and rearranging terms gives

$$\text{Var}(S) = \text{Var}(E) \sum_{j=\infty}^{+\infty} g^2(t_j). \tag{99}$$

Note that because the positive and negative lobes of the signal must balance charge,

$$\sum_{j=-\infty}^{+\infty} g(t_j) = 0.$$

This implies through Eq. (93) that $\langle S \rangle = 0$, so that the average signal is zero, as is required for baseline restoration. In addition, a fixed amplitude energy deposition will have $\mathrm{Var}(E) = 0$ so that the variance of S will also be 0. Thus, a constant energy deposit will not appear in the shaped signal.

References

[1] A. Papoulis, Signal Analysis (McGraw-Hill, 1976) p. 324.
[2] V. Radeka, Ann. Rev. Nucl. Sci. 38 (1988) 217.
[3] E.G. Stern, E_t Fluctuations in Pileup Events as a Function of Pseudorapidity, GEM Technical Note 92-111 (June 1992) p. 503 (unpublished).
[4] W.E. Cleland, E.A. Scholle and E.G. Stern, Symp. on Detector Research and Development for the Superconducting Supercollider, Ft. Worth, Texas, 1990, p. 318.
[5] W.E. Cleland and E.G. Stern, Proc. 3rd Conf. on Calorimetry, Corpus Christi, Texas, 1992.
[6] R.R. Chase, C. de La Taille, S. Rescia and N. Seguin, Nucl. Instr. and Meth. A 330 (1993) 228.
[7] V. Radeka and S. Rescia, Nucl. Instr. and Meth. A 265 (1988) 228.
[8] N.R. Campbell, Proc. Cambridge Philos. Soc. 15 (1909) 117.
[9] F.N.H. Robinson, Noise and fluctuations in electronic devices and circuits (Clarendon, Oxford, 1974) p. 15.
[10] C.W. Fabjan, in: The Feasibility of Experiments at High Luminosity at the Large Hadron Collider, CERN 88-02 (1988) p. 19.
[11] A. Yamashita and K. Kondo, in: Physics of the Superconducting Supercollider, Snowmass 86 (1986) p. 365.
[12] G.O. Halverson and J. Huston, ibid., p. 368.
[13] P.T. Cox, in: The Feasibility of Experiments at High Luminosity at the Large Hadron Collider, CERN 88-02 (1988) p. 25.
[14] J. Freeman and C. Newman-Holmes, Proc. Workshop on Detector Simulation for the SSC, ANL-HEP-CP-88-51, ed. L. Price, Argonne National Labs, (1988) p. 285.
[15] R.K. Bock et al., Nucl. Instr. and Meth. 186 (1981) 533.
[16] W.E. Cleland and A.V. Vanyachin, GEM Technical Note TN 93-376, April 1993 (unpublished).
[17] E. Gatti et al., Nucl. Instr. and Meth. A 274 (1989) 469.
[18] W.J. Willis and V. Radeka, Nucl. Instr. and Method. 120 (1974) 221.